HOMOGENEOUS CATALYST MEDIATED GLUCOSE MUTAROTATION STUDIES USING VIBRATIONAL SPECTROSCOPY

By

PRANAV RAMESH

A thesis submitted to the

Graduate School- New Brunswick

Rutgers, The State University of New Jersey

in partial fulfilment of the requirements

for the degree of Master of Science

Graduate program in Chemical and Biochemical Engineering

Written under the direction of

Dr. George Tsilomelekis

and approved by

_____

_____

_____

New Brunswick, New Jersey

October, 2017

ABSTRACT OF THE THESIS

HOMOGENEOUS CATALYST MEDIATED GLUCOSE MUTAROTATION STUDIES USING VIBRATIONAL SPECTROSCOPY

By PRANAV RAMESH

Thesis Director:
George Tsilomelekis

The pitfalls of overdependence on fossil fuels are well documented. Current research aims to focus on biomass obtained from renewable cellulose for the production of fuels and chemicals. In that regard, with cellulose as source, 5-hydroxymethylfurfural (HMF) is a versatile platform chemical for the production of chemicals like levulinic acid. The isomerization of glucose to fructose is one of the steps in the synthesis of HMF from cellulose. Glucose exists in several anomeric forms and it has been shown that the isomerization reaction is anomer specific. This work focuses on the study of mutarotation in glucose in the presence of homogeneous Lewis acid catalysts.

A combination of spectroscopic tools: ATR-IR and Raman spectroscopy are used to study the vibrational modes of glucose in aqueous solution. At room temperature, changes in vibrational modes can be attributed to the mutarotation reaction. This work compares the rate of mutarotation in different concentrations of $AlCl_3$, $CrCl_3$ and $SnCl_4$. The influence of metal salts in solution, pH and ionic strength were also probed by comparing with the rates obtained in Brönsted acids. The mutarotation in Lewis acid is faster than that in water. It is fastest in $SnCl_4$ and increases with increase in concentration of $SnCl_4$. Results also indicate a lack of glucose-Lewis acid interactions. However, rates vary depending on the nature of metal salts in solution indicating that the mutarotation is influenced by the nature of Lewis acid-water interactions.

Acknowledgements

I would like to express my heartfelt gratitude to Dr. George Tsilomelekis for his guidance and support in my research. He has made me an infinitely better researcher and instilled in me the importance of questioning everything.

I would also like to thank Shreyas Acharya for all the quality discussions we have had. I extend my thanks to my colleagues Trang Tran, Hualin Qiao, Jiazheng Zhou, Yusheng Guo, Ayman Saleh and Amit Patel for their support.

I thank my friends Vijaydev Ganesan, Chandra Kanth Bandi, Pruthvi Jujjavarappu, Bharathram Molakala and Varsha Rane for their encouragement.

I am forever indebted to my parents, my grandparents and my sister for their love and support.

Table of Contents

List of Tables

List of Figures

CHAPTER 1

INTRODUCTION

The search for clean source of energy and chemicals has never been more important considering the vagaries of political and economic consequences of petroleum dependency. In this regard, 5-hydroxymethylfurfural (HMF) offers a versatile and clean platform for the production of a variety of chemicals from biomass.

The formation of biomass can be best summarised as follows:

$$CO_2 + H_2O \rightarrow (CH_2O)_x + O_2$$

Biomass comprises of 3 constituents: cellulose, hemicellulose and lignin. The overall composition of biomass is approximately:

- 77-90% by weight sugar polymers
- 10-25% by weight lignin

The decomposition of the three major constituents yields the same major gases: CO_2, CH_4 and CO indicating similar chemical composition..

Cellulose and hemicellulose can be converted to ethanol directly by fermentation (1) (2) (3) (4) and lignin to chemicals by pyrolysis (5), gasification (6) and more recently by bacterial action (7).

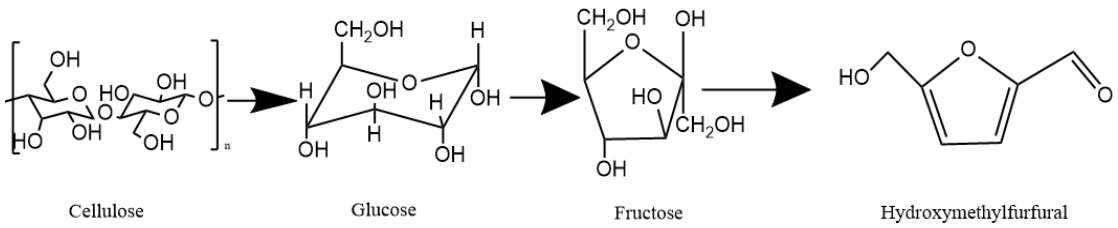

Figure 1: Schematic model for synthesis of HMF from cellulose

Cellulose undergoes hydrolysis to yield glucose. HMF can be produced directly from glucose via dehydration or through glucose isomerization to fructose followed by dehydration to HMF. The direct conversion of glucose to HMF results in decreased conversions and increased formation of side products (8) (9) (10).

Cellulose possesses a crystalline structure with strong inner beta-1,4-glycosidic bonding and a complex hydrogen bonded network making its hydrolysis difficult (11). The isomerisation of glucose to fructose suffers from difficulties in conversion of glucose which exists predominantly as a 6-membered ring to fructose which exists as a 5-membered ring in solution.

Industrially, the isomerization reaction is carried out by the enzyme *glucose isomerase* (12). The use of enzymes for this step makes the reaction susceptible to limitations of temperature and purity and makes the (enzymatic) reaction unsuitable for one-pot

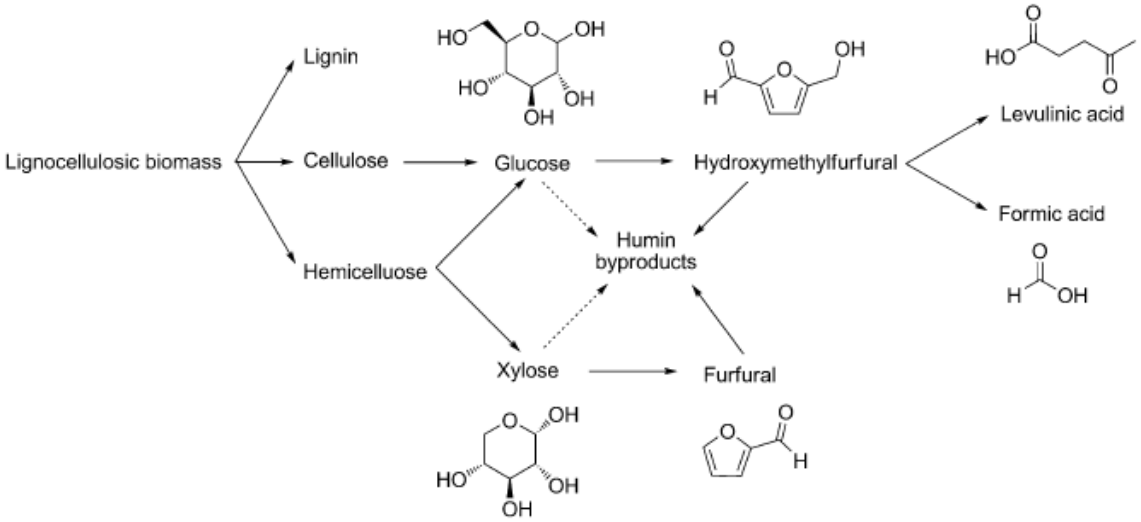

Figure 2: Byproducts in conversion of biomass to HMF (82)

conversion to HMF. Lewis acids have been reported to catalyze the isomerization reaction (13) (14) and consequently have been incorporated with a combination of Brönsted acid for one-pot synthesis of HMF from glucose (15) (16)

An aqueous solution of glucose consists of several tautomers: alpha-D-glucopyranose, beta-D-glucopyranose, alpha-D-glucofuranose, beta-D-glucofuranose and the open chain glucose. It has been reported that the presence of specific anomers has an effect on the kinetics of isomerisation. For the enzymatic reaction, conversion rate was 43% higher with alpha-D-glucose compared to equilibrated glucose (34% alpha and 66% beta) and 113% higher compared to beta-D-glucose (17). Hence, greater the percentage of alpha-D-glucose in solution, the more efficient is the isomerization reaction. This makes the study of transformation of glucose anomers (mutarotation) critical which is undertaken in this thesis. Mutarotation is the change in optical rotation because of the change in equilibrium between two anomers. In addition to studying the mutarotation reaction in water, this thesis also focuses on this mutarotation reaction in Lewis acids. Attention is paid to Lewis acids since these compounds have been shown to catalyze the isomerization reaction and significant differences in catalytic activity has been reported for the

isomerization of glucose to fructose in the presence of $AlCl_{3,}$ $CrCl_3$ and $SnCl_4$ (18) with highest selectivity reported for $AlCl_3$ (82.7%) while highest conversion was reported with $CrCl_3$ (52.3%). Consequently, based on the calculated rate constants, the rates for isomerization reaction follow the order: $CrCl_3 > AlCl_3 > SnCl_4$.

1.1 Goals

1. Study variations in mutarotation kinetics of glucose as a function of nature and concentration of different metal salts
2. Shed light on the glucose-water-metal salt interactions.
3. Understand the effect of speciation of metal salts on the mutarotation

CHAPTER 2

BACKGROUND

2.1 Mutarotation in glucose

An aqueous solution of glucose consists of the open chain glucose, alpha and beta anomers in the pyranose (6 membered ring) and furanose (5 membered ring) form. The pyranose form exist predominantly in solution. The conversion of the alpha to the beta form or vice versa is termed as mutarotation.

The study of anomers of glucose in solution was carried out by polarimetry (19). This was based on the different degrees by which the tautomers rotated plane polarized light (+18.7 degrees for beta-glucose and +112.2 degrees for alpha-glucose). An equilibrated glucose solution consists of 66% beta-glucose and 34% alpha-glucose with (+52.7 degrees).

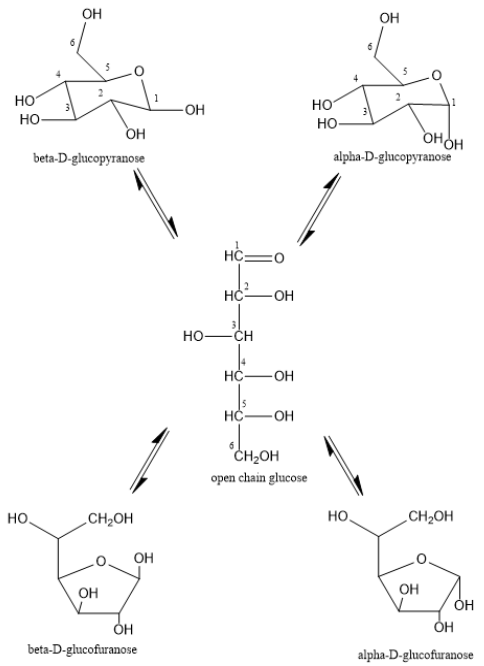

Figure 3: Tautomers of glucose in solution

Several mechanisms have been proposed for the mutarotation in glucose. They can be broadly classified into endocyclic oxygen attack and the exocyclic oxygen attack. The most accepted mechanism is the endocyclic oxygen attack which involves the formation of the open chain glucose. The exocyclic oxygen attack involves intramolecular proton transfer and attack on the O1 atom. Rittenberg and Graff (20) demonstrated that the attack on the O1 atom is 30 times slower than the mutarotation reaction. This indicates that reaction proceeds by exocyclic oxygen attack. The mechanism of glucose mutarotation involves the following steps for the endocyclic route (21) (22):

1. Protonation of the endocyclic oxygen
2. O1-H bond breakage
3. O5-C1 bond breakage leading to the open chain glucose
4. Rotation across C1-C2

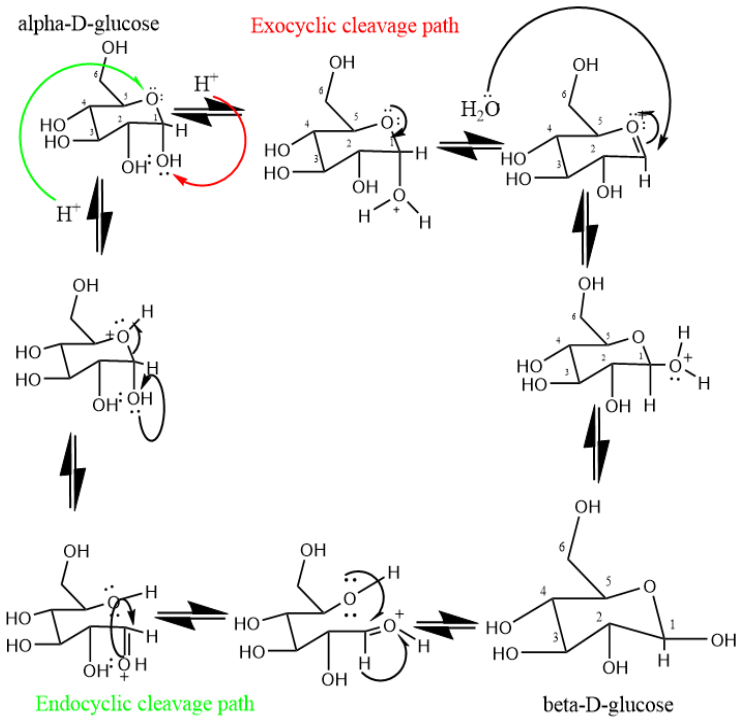

Figure 4: Mechanism of endocyclic acid catalyzed glucose mutarotation (23) (24)

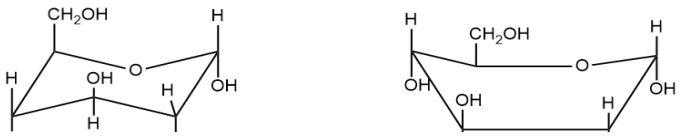

Figure 5 : Boat and chair conformers of glucose

Both chair and boat conformers of alpha-D-glucopyranose exist in equilibrium. The chair form is more stable than the boat form as heavier atoms are farther away from each other. It is for the same reason that beta-D-glucopyranose is more stable compared to alpha-D-glucopyranose.

Due to the ubiquitous nature of sugars, especially glucose, a wealth of literature is available on the effect of solvents, acids and temperature on the mechanism of mutarotation. Tanret in 1896 demonstrated the presence of anomers of glucose by isolating alpha-anomer, beta anomer and also a third glucose structure, which could not be identified with available methodology, which could be converted to beta-glucose in aqueous media. The differences were established using polarimetry. However it was later established that the third form was merely a combination of the alpha and beta anomers in equilibrium. It should not be overlooked that Tanret's original analysis does not take into account a reversible reaction that takes place leading to the existence of the two anomers in equilibrium. Crystallization of glucose from an aqueous solution leads to the formation of the alpha-anomer which would not be possible if Tanret's irreversible reaction hypothesis was true. Further study of mechanism indicated that the conversion would be impossible without the formation of the aldehyde or hydrate as an intermediate. This led to the study of the open chain glucose which was Tanret's postulated third glucose structure. It should

be noted that several contemporaries of Tanret(Ber.,1896,29,203) regarded complete conversion to isomeric aldehyde form (the third anomer).

Lowry (23) studied the effect of acid and alkali on the mutarotation of glucose using polarimetry. The rate of mutarotation was found to be directly proportional to the square root of acid concentration and directly proportional to the concentration of alkali (23). This may indicate that the ionic strength might significantly affect the mutarotation rates. The effect of ionic strength on the mutarotation rates in the presence of Lewis acids has been studied in this work. The results of Lowry's experiments are described in Figure 6. Lowry (23) therefore observed slight acceleration in N/100 HCl whereas equilibrium was achieved in 30 minutes. Using N/1000 caustic potash, in comparison, it took 3 hours for equilibrium to be achieved using N/100 HCl solutions.

The rate constants have also been determined for the mutarotation of glucose using

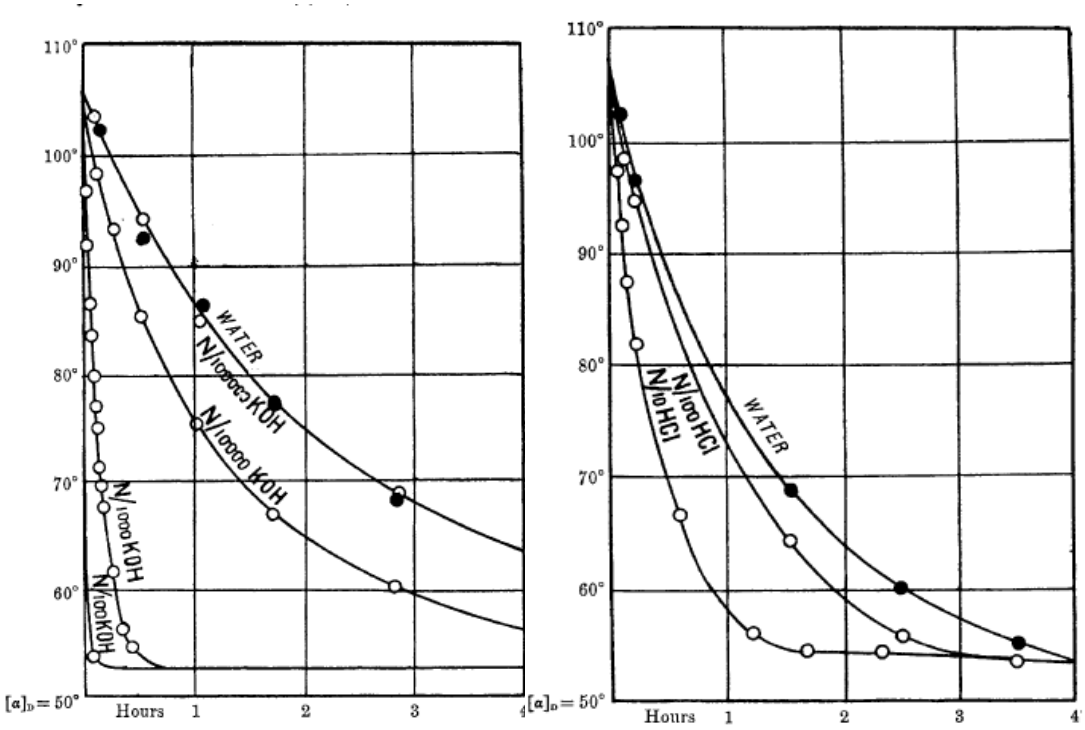

Figure 6: Effect of acid and alkali on mutarotation of glucose (25)

several experimental methods- polarimetry (24) (19) (25), spectroscopy and even blood glaucometry (26). The conversion of alpha-glucose to beta-glucose follows pseudo first order kinetics with equilibrium percentages at 36% alpha-glucose and 64% beta-glucose. Similar studies have also been undertaken in frozen solutions wherein the acid catalyzed mutarotation was reported to be faster than the same at room temperature (27). Other

studies include the study of mutarotation in mixtures of solvents (28) (29). Moreover, interactions between glucose and water molecules have also been probed in theoretical work by Shinichi Yamabe (30). Shinichi Yamabe assumed two imaginary transition states wherein the alpha-D-glucose underwent intermolecular hydrogen bonding leading to the formation of a network where one alpha-D-glucose molecule bonds to **n** number of water molecules (where **n**=1,2 and 3 refers to the number of water molecules bonded to glucose) where a four centred reaction centre TS1 is formed. The TS1 transforms to the aldehyde form which is then converted to a four centred transition state TS2 by ring closure leading to the formation of the beta-anomer in the next step. The relative energies of activation are summarized in Table 1. Activation energy decreases as **n** increases for both alpha and beta anomers indicating that dimmers and trimers of water bonded very strongly with glucose.

	Activation Energy (in kcal/mole)					
Number of water molecules (n)	**Alpha form**	**Alpha form bonded to n water molecules**	**Transition State 1 (TS1)**	**Aldehyde bonded to n water molecules**	**Transition State 2**	**Beta form bonded to n water molecules**
0	0	0	+50.84	+12.00	+49.19	+2.07
1	0	-8.20	+22.62	3.60	+20.97	-7.94
2	0	-13.25	+15.98	-2.55	+14.34	-12.09
3	0	-21.69	+3.19			

Table 1: Relative activation energies (32)- Negative values indicate greater stability

2.2 Isomerization of glucose to fructose

The conversion of glucose to fructose by isomerisation is considered a very important step for the conversion of cellulosic biomass to chemicals and fuels. Although direct conversion of glucose to HMF can be achieved, synthesis of HMF from fructose is advantageous owing to the fact that fructose predominantly exists in the form of five member rings in sharp contrast to glucose which exist in the form of six member rings. Apart from its use for the synthesis of HMF, fructose is also used to produce sweeteners for the food industry. However, the direct use of fructose to make the aforementioned products possesses an important drawback: the cost of fructose. For this reason, the use of

less costly cellulose derived glucose provides an important alternative for the implementation of the biorefinery concept. Commercial isomerisation of glucose to fructose is achieved by the enzymatic route with *glucose isomerase* acting as the enzyme (31). Further, continuous conversion of glucose to fructose using immobilized enzymes has also been achieved (32). More importantly, it was observed that the reaction is anomer specific: (33) (31) demonstrated that this reaction is alpha-anomer specific.

The first reported isomerisation of glucose was in 1885 with the reaction catalyzed by a base (34). (35) studied the isomerization of glucose to fructose using sodium hydroxide and calcium hydroxide at room temperature. The drawback of this method was poor yields and the large amounts of acidic by products formed which neutralized the base used. This was replaced by organic amines (triethylamine) (36) with the added advantage being slower degradation of saccharides. Further research on utilization of bases as catalysts for the isomerisation led to the use of borates, boronates and aluminates (37) (38) which were found to considerably increase the yield of this reaction. This was attributed to the greater tendency of formation of complexes between anions of borates (boronates and aluminates) with fructose compared to glucose which in turn stabilized fructose and further shift the equilibrium towards the favourable product. Solid bases resemble soluble bases kinetically with examples including KOH, cation exchanged zeolites and magnesium-aluminum hydrotalcites. The mechanism for base catalyzed isomerization reactions was put forth by Carraher et al (39).

The mechanism is depicted in Figure 7 and can be summarized as follows: 1) Formation of glucose anion due to attack by hydroxide ions leading to the formation of open chain glucose. 2) Abstraction of hydrogen atom from C2 to ene-diol intermediate. 3) Formation of open chain fructose. 4) Protonation of open chain fructose which leads to complete fructose.

The isomerization reaction was carried out in aqueous media. Metal salts coordinate with water leading to deactivation of the catalyst. For this reason, the study of mutarotation reaction catalyzed by Lewis acids lagged behind bases. The coupling of Lewis with Brönsted acids enables one pot synthesis of HMF from glucose which is considered as an advantage. Commonly used metal salts such as $CrCl_3$, $AlCl_3$ and $SnCl_4$ have been reported by Tang et al as effective isomerization catalysts; their catalytic activity

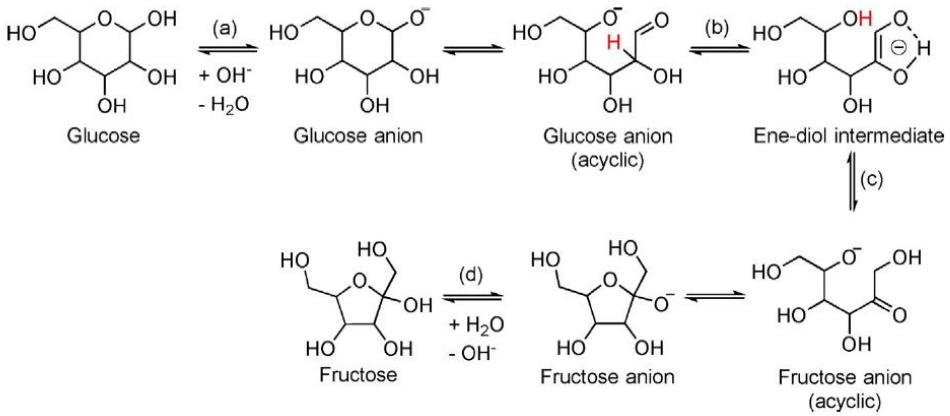

Figure 7: Mechanism of base catalyzed isomerization reaction with amines (39)

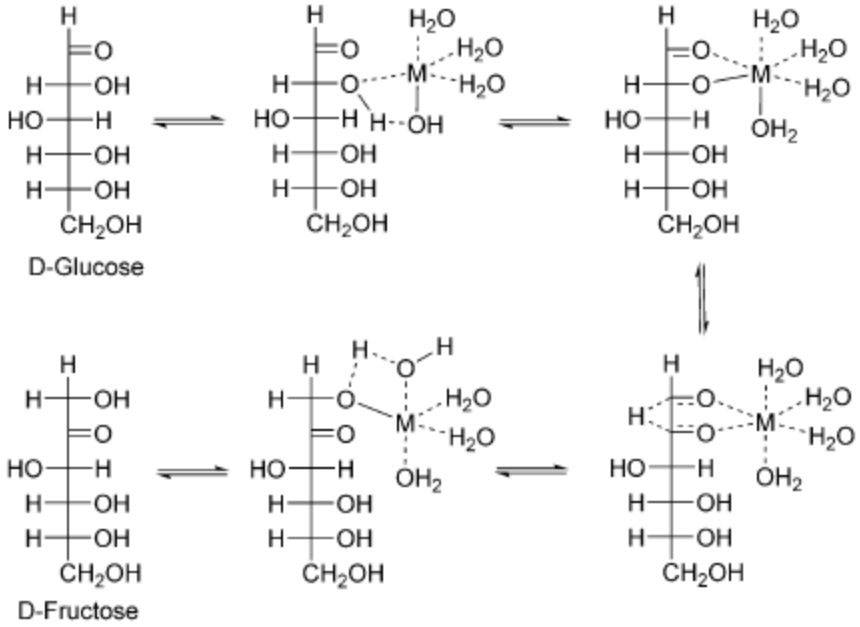

Figure 8: Mechanism for isomerization reaction catalyzed by a Lewis acid (41)

decreases in the order $CrCl_3$> $AlCl_3$ > $SnCl_4$ (40). Further, the species responsible for isomerisation have also been explored for $CrCl_3$: $[Cr(H_2O)_5(OH)]^{2+}$ (41) and for $AlCl_3$:$[Al(OH)_2aq]^+$ (40). In addition to soluble Lewis acids, solid catalysts have also been reported for the isomerization reaction. Most common acid catalysts include Sn-beta zeolites and Ti-beta. The mechanism for the acid catalyzed isomerisation reaction is summarized in Figure 8.

2.3 HMF

5-hydroxymethylfurfural (HMF), in recent years, has been touted as a potential platform chemical for the production of fuels and chemicals from biomass. HMF can be used as a building block chemical for the synthesis of among other chemicals, biofuel 2,5 dimethylfuran(DMF) (42) (43) (44)and monomer 2,5 furandicarboxylic acid (45) (46). HMF can undergo reactions pertaining to the hydroxy methyl group, the formyl group and the furan ring. Ketoses, namely fructose is a better starting material for the synthesis of HMF compared to aldoses (glucose). This is due to the fact that glucose forms stable 6-membered rings in solution which is thermodynamically unfavourable to undergo dehydration to HMF directly. Fructose forms less stable ring structures thereby a greater proportion exists in the open chain form which aids the enolisation rate (rate determining step). The conversion of fructose to HMF has been achieved by homogeneous and heterogeneous catalysts. Examples include H_2SO_4, HCl and H_3PO_4 (47) (48) in addition to Lewis acid such as $ZnCl_2$ and $AlCl_3$ (49) (50). Examples of heterogeneous catalysts for the dehydration of fructose to HMF include TiO_2 (51) and ZrO_2 (51) and Ce-phosphates (52). Kuster (53) compiled a list of factors determining the rate of formation HMF from cellulose:

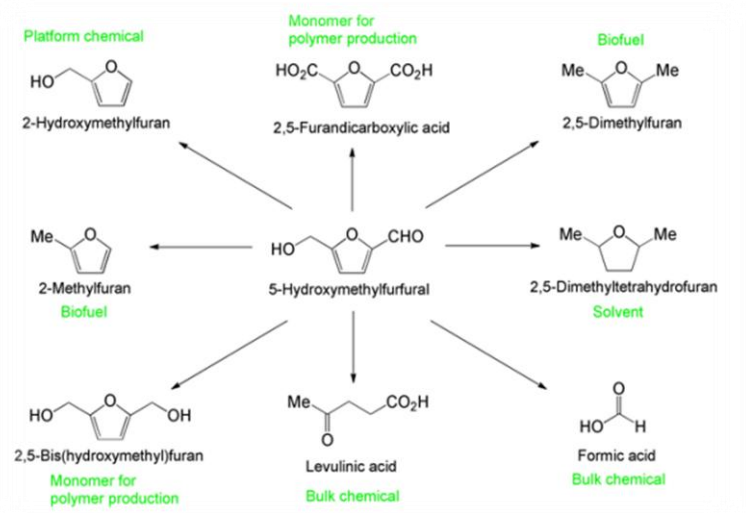

Figure 9: HMF as a platform chemical

1. Substrate (aldoses or ketoses)
2. Type and concentration of catalyst
3. Time and temperature
4. Presence of solvent

2.4 Lewis acid catalysts

Broadly, Lewis acids are electron acceptors. This definition by Lewis was very general and was postulated based on the kinetics of the neutralisation process. Hence, Lewis classified acids into primary acids and secondary acids (54). Primary acids are those acids which have zero activation energy when reacted with primary bases. This puts together acids whose acid properties appear immediately. Alternatively, secondary acids include those acids which require activation energy before the acid properties are revealed.

Pearson (55) put forth a new concept called Hard and Soft Acid and Bases (HSAB) with hard acids being defined as small sized, positively charged and unpolarizable electron acceptors. They concluded stating that hard acids interact with hard bases and vice versa with respect to soft acids. More recent methods to understand quantitatively, based on the charge controlling effect the Lewis acidity has been based on perturbation molecular theory (56) and density functional theory.

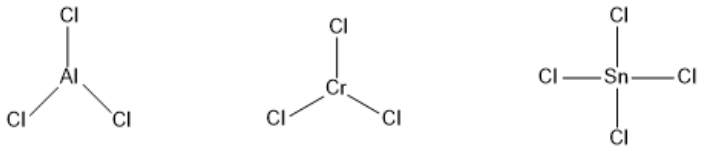

Figure 10 : Structure of Lewis acids

Metal atoms bonded to highly electronegative species are typical examples of Lewis acids. The central metal atom acquires a partial positive charge thereby attracting electron pairs. Further, transition elements are capable of expanding their octet to accommodate electrons. More importantly, the non-metal to which the central metal atom is bonded to decides the acid strength.

Lewis acids are used to catalyze a wide range of reactions including but not limited to:

1. Formation and hydrolysis of acetals
2. Alkene alkylation
3. Alkene dimerization
4. Friedel Craft's reaction
5. Oxidation reactions

In order to explain the effect of Lewis acids in water, a basic overview of the water molecule is required. Spectroscopy of water in 1977 revealed the presence of water dimers (57). More recent ab-initio calculations predicted the existence of large water

clusters-trimers, tetramers and pentamers of water- each monomer acts as a single acceptor and a single donor (58). The calculations were based on increasing the maximum number of hydrogen bonds possible while simultaneously decreasing the molecular strain. It was observed that for larger clusters-hexamers of water there was a tendency to form 3D structures (59). These structures have been analyzed using a combination of Monte Carlo calculations and far-IR laser vibration tunnelling spectroscopy (60). Addition of Lewis acids to water disrupts this hydrogen bonded structure. Shu Kobayashi described a correlation between catalytic activity in water and hydrolysis constants and exchange rate constants (61). Based on their findings, they proposed a mechanism wherein, metal ions (cations) dissociate in water from corresponding compounds and hydration of these metal ions occurs immediately. At this stage, intermolecular and intramolecular exchange reactions of water molecules occur. It was established that Lewis acids with hydrolysis constants between 4.3 to 10.08 and Water Exchange Rate Constants greater than $3.2X10^6$ $M^{-1}s^{-1}$ were best catalysts for the Mukaiyama aldol reaction. This was attributed to the stability of cations. Greater the hydrolysis constant, greater is the stability of cations. WERC is related to $(electron)^2$/Ionic Radii. A small $(electron)^2$ /Ionic Radii means faster WERC. The bounds for hydrolysis constants were established since high stability corresponds to poor catalytic activity. The effect of addition of alkali metal halides (62) and dissolved halides (63) on hydrogen bond network of water has also been studied. The nature of Lewis acids used- combination of cation and anion present can alter the nature of hydrogen bonding in water in different ways.

The hydration of complex species in solution (64) can be approximately written as:

$$xM^{2+} + y\,H_2O \rightleftharpoons M_x(OH)_y^{(xz-y)+} + y\,H^+$$

Ligand formation with increasing charge to ratio of cation is: $H_2O < OH^- < O^{2-}$.

Cation	**Al^{3+}**	**Cr^{3+}**
WERC ($M^{-1}s^{-1}$)	1.6	5.8×10^{-7}
Hydrolysis Constant	4	1.14

Table 2: WERC and hydrolysis constant for Lewis acids under consideration

2.5 Vibrational Spectroscopy

Spectroscopy deals with the interaction of electromagnetic radiation with matter. Electromagnetic radiation is a form of energy comprising of alternating electric and magnetic fields acting in planes perpendicular to each other and the direction of propagation. These radiations are produced as a consequence of oscillators arising from the acceleration of electric charges. There are two theories by which the impact of electromagnetic radiation can be explained: Classical theory and Quantum Theory. Maxwell's Classical Theory considers radiation *as 2 mutually perpendicular electric and magnetic fields in a single plane at right angles to each other in phase propagated as a continuous sine wave*.

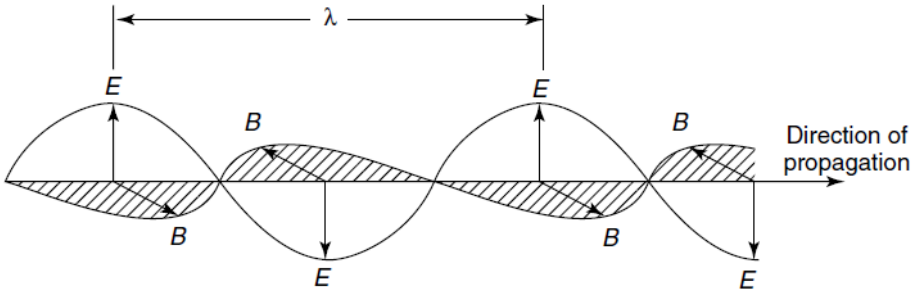

Figure 11: Propagation of Electromagnetic wave (70)

From the classical theory,

$$c = \lambda\nu$$

c is the velocity of propogation which is constant in vacuum ($3x10^8$ m/s)
λ is the wavelength of radiation (m)
ν is the frequency (1/s)

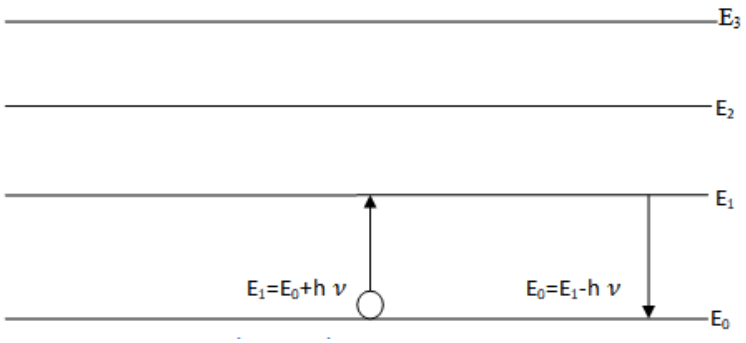

Figure 12: Discrete Energy levels

Typically, the term wavenumber ($\tilde{\nu}$) is used in spectroscopy which is the inverse of wavelength which offers the advantage of being linear with energy.

$$\tilde{\nu} = \frac{1}{\lambda} = \nu/c$$

However, a series of experiments by Bohr, Plank and Einstein indicated that it would be disingenuous to consider electromagnetic radiation interaction with matter as continuous which led forth to the quantum theory. Quantum theory proposes the existence of discrete energy levels. Every atom or molecule exists in these discrete energy levels and interaction with electromagnetic radiation leads to a quantum increase in energy which exactly fits the energy gap. The corresponding energy (in Joules) according to quantum theory is best expressed by the equation:

$$E = h\nu$$

Where h is Planck's constant ($6.626X10^{-34}$ Js) and ν is the classical frequency (1/s)

In a molecule, atoms are distributed among various energy levels. Atoms must absorb radiation exactly equal to the energy gap in order to jump to the next energy state. Hence the frequency required for transmission is given by:

$$\nu = (E_1 - E_0)/h$$

2.6 IR Spectroscopy

IR spectroscopy involves impinging matter with Infrared radiations and measuring the quantity of incident radiations absorbed by the sample. Primitive IR instruments were primarily dispersive instruments consisting of prisms which were replaced by dispersive gratings in the 1950's. However, real progress in the use of IR spectrometers arrived with the use of Fourier Transform Spectrometers and corresponding increase in computational power. For a molecule to be IR active, the dipole moment of the molecule must change during vibration. This is a necessary condition for IR activity. This renders IR spectroscopy a convenient tool for the study of heteronuclear molecules. Homonuclear molecules are IR inactive. Let us consider two simple heteronuclear molecules: linear CO_2 and non-linear depicted in figure 13. Hence for a linear molecule, the number of vibrational modes is given by 3N-5. Figure 15 depicts the vibrational modes of water. A- Symmetric stretching mode where both OH bonds contract and expand in phase; B- asymmetric stretching mode where one OH bond

Figure 13: Molecular structure of water and carbon dioxide

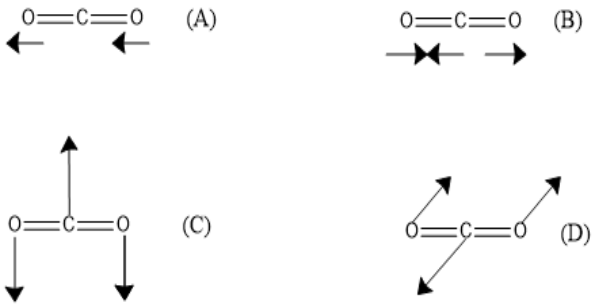

Figure 14: Vibrational modes of carbon dioxide

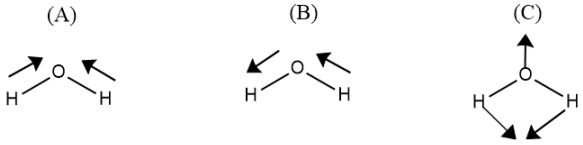

Figure 15: Vibrational modes of water

expands while the other contracts; C- (scissoring)bending mode where oxygen and hydrogen atoms move out of plane.

Hence, for a non linear molecule, the number of vibrational modes is given by 3N-6. In the above cases, vibrations can be due to change in length of bonds or as a consequence of one atom moving out of its current plane- classified as stretching and bending modes respectively. 4 vibrational modes are possible for carbon dioxide described in figure 14 where: A- symmetric stretching mode where both CO bonds contract and expand in phase; B- asymmetric stretching mode where one CO bond expands as the other contracts; C and D- bending modes where carbon and oxygen atoms move out of the current plane with the difference between the modes only being the direction in which said movement takes place.

It should be noted that variations in dipole moment are profound in asymmetric stretching modes only- hence these are IR active whereas the net dipole moment of symmetric stretching modes is zero and hence are IR inactive.

Moreover, bonds between similar molecules lead to poor absorption (due to lower dipole moments).

The IR source typically emits IR radiation of all frequencies in the range of study. This could be near IR (14000-4000 cm^{-1}), mid IR (4000-400 cm^{-1}) or far IR (400-10 cm^{-1}). IR radiations are absorbed by a molecule if there is a change in the dipole moment. An IR spectrum is a plot between absorbance (reflectance or transmittance) versus the wavenumber. The wavenumber is a measure of the energy difference between the ground state and excited (vibrational) state. The intensity of the IR band measured is proportional to the square of the change in dipole moment. The relationship between absorbance and the concentration of a sample is given by Beer Lambert's law.

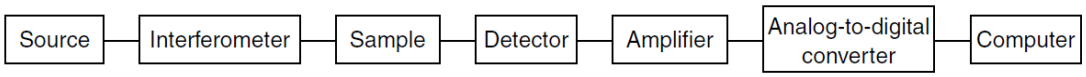

Figure 16: Components of a FTIR spectrometer (87)

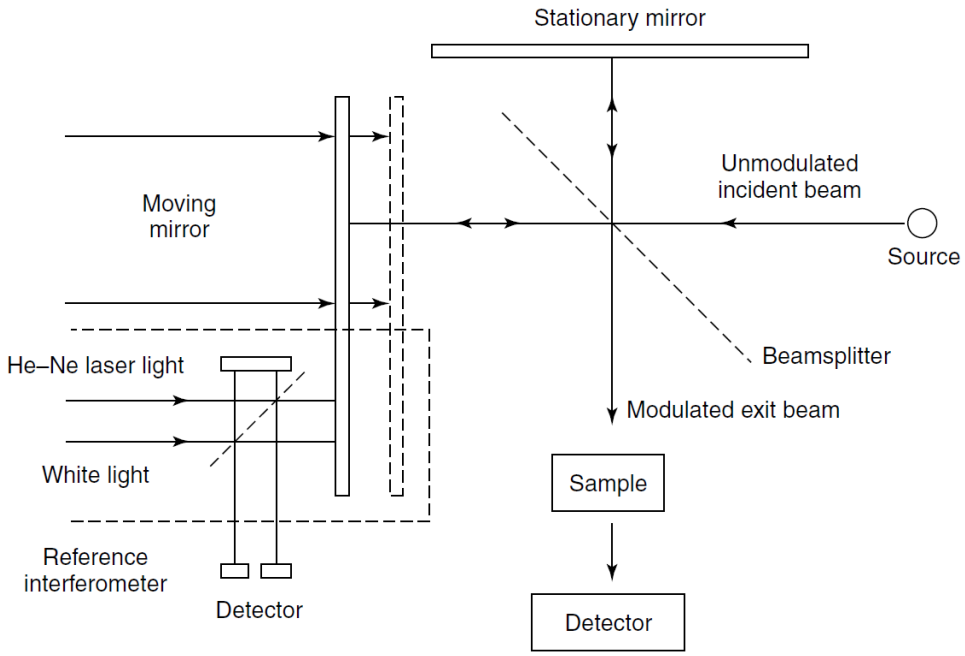

Figure 17: Michelson Interferometer

2.6.1 Instrumentation

The source of IR radiation commonly used is Globar or Nernst source. The former is a silicon carbide rod which is electrically heated up to 1650^0 C whereas the later is a tube consisting of certain oxides of zirconium, yttrium and erbium heated to 2000^0 C.

Michelson interferometer is the most common of its type and consists of two plane perpendicular mirrors- a stationary mirror and a moving mirror. Additionally, it consists of a beam splitter which splits incident beam into two parts. One part passes onto the moving mirror and the other part into the stationary mirror. Half the beams falling on the respective mirrors are reflected back into the beam splitter where they combine. Half the beam from the stationary mirror is transmitted through the beam splitter and the other half to the source. The output beam from the interferometer (perpendicular to incident beam) is used for analysis.

The objective of a moving mirror is to produce a path difference and constructive interference takes place for the reflected beams. The output beam from interferometer

passes through the sample and then onto the detector. The most common detector is the DTGS (Deuterium Tryglycine Sulfate). Greater sensitivity is achieved using an MCT (Mercury Cadmium Telluride) which however requires cooling to liquid nitrogen temperatures.

2.6.2 Attenuated Total Reflectance

ATR is one of two commonly used sampling techniques from reflection- the other being DRIFTS (Diffuse Reflectance Infrared Fourier Transform Spectroscopy). ATR is a contact sampling technique. ATR utilizes a crystal of high refractive index and IR

IR radiation falling on a sample can be reflected (I_r) , absorbed (I_a), transmitted (I_t) or scattered (I_s). This is given by:

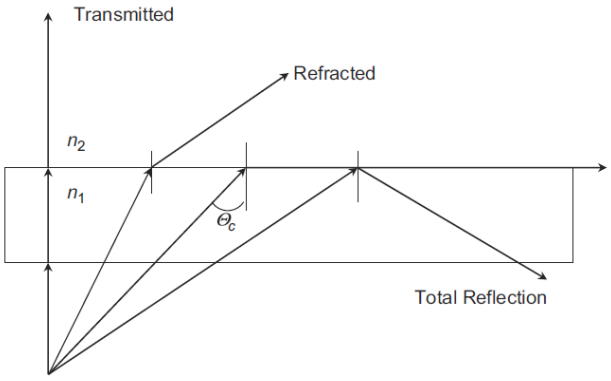

Figure 18: Incident radiation at an interface (88)

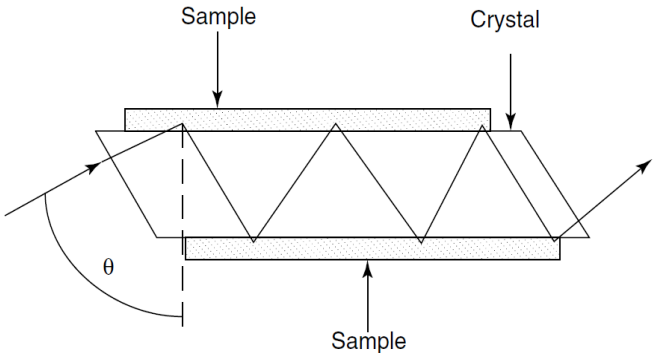

Figure 19: Total Internal Reflectance (89)

$$I = I_a + I_t + I_r + I_s$$

Hence any of the above parameters can be used to get sample information.

In ATR, the reflected light provides information at the sample-crystal interface. The choice of material for the crystal is vital to ensure total internal reflectance occurs since the critical angle is a function of refractive index of sample and the crystal. Diamond, Germanium and ZnSe are commonly used crystals. ATR is particularly useful for thick samples as well high absorbing samples.

2.7 Raman Spectroscopy

Raman spectroscopy involves impinging the sample with monochromatic radiation from a laser in the UV, visible or near IR range and measuring the scattered radiation using a spectrometer.

Consider incident radiation of frequency ν_L on a molecule. This leads to transmission, absorption and scattering of the incident radiation. The incident radiation causes excitation of the molecule to a virtual state. The virtual state can be described as a temporary short lived state after which the molecule returns to the ground state. Most of the scattered radiation has the same frequency as that of the incident radiation. However some of the scattered radiation possesses frequency of magnitude $\nu_L + \nu_m$ or $\nu_L - \nu_m$ where ν_m depends on the transitions between the vibrational, translational and electronic energy levels of the molecule. If the scattered radiations have the same frequency as incident radiation, the phenomenon is called Rayleigh scattering whereas variations in frequency of incident and scattered radiation are termed as Raman scattering. This scattering occurs in all directions and observed intensity is dependent on direction of observation. Further, frequency of magnitude $\nu_L + \nu_m$ is referred to anti-Stoke's band whereas frequency of magnitude $\nu_L - \nu_m$ is referred to as Stoke's band. This is summarized in Figure 20.

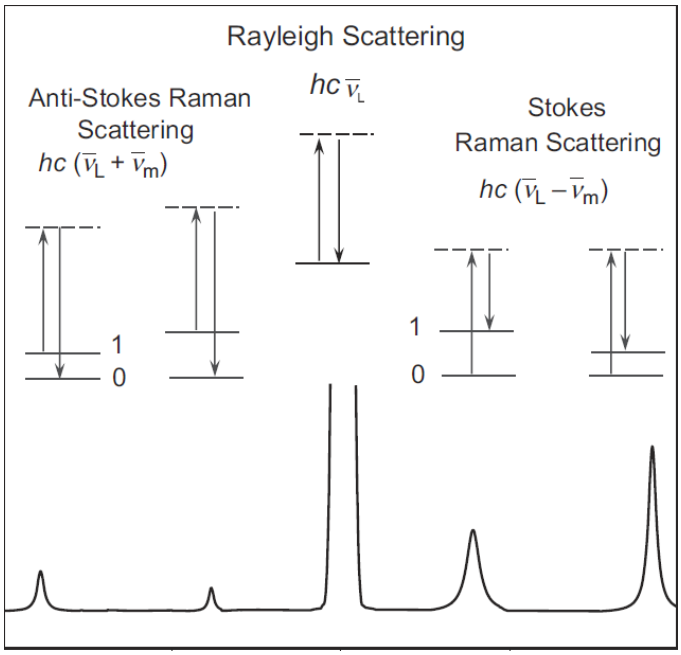

Figure 20: Rayleigh, Stoke's and anti-Stoke's scattering (89)

Rayleigh scattering is the most probable event and the observed intensity of scattered light for Raman scattering is 10^{-6} times smaller. It should be noted that the ground state is more populated than excited levels and hence the Stoke's scattering is more intense than the Anti-Stoke's scattering. Further, less than 0.001% of incident radiation

undergoes Raman scattering. Moreover, Stoke's lines are usually used in the spectra due to its higher intensity.

An oscillating electric field is given by:

$$F = F_0 \cos(\nu_0 t)$$

This electric field induces a dipole moment in a molecule given by:

$$\mu = \alpha F_0 \cos(\nu_0 t)$$

Where α is the polarizability of a molecule and is given by:

$$\alpha = \alpha_0 += \sum_{m=1}^{M} \alpha_0 \cos(\nu_m t + \Phi_m)$$

$$P = \alpha F_0 \cos(\nu_0 t) + \sum_{m=1}^{M} \alpha_m \cos((\nu_0 + \nu_m) t + \Phi_m) + \sum_{m=1}^{M} \alpha_m \cos((\nu_0 - \nu_m) t + \Phi_m)$$

Hence, for a molecule to be Raman active, the polarizability must change during vibration. Consider a molecule in an electric field- a dipole moment is induced in the molecule as electrons are attracted to the positive pole and positively charged nuclei towards the negative pole. Hence IR and Raman spectroscopy can be used to obtain complementary information about a molecule.

The Raman intensity is dependent on several parameters and can be best summarized by the equation:

$$I_R = \nu^4 I_0 N \left(\frac{\partial \alpha}{\partial Q}\right)$$

Where ν is frequency of laser used, I_0 is intensity of incident beam, N is number of scattered molecules, α is polarizability and Q being vibrational amplitude.

2.7.1 Instrumentation

Raman spectrometers typically consist of a laser excitation source, collection optics, a monochromator (or interferometer) and a detector.

It should be noted that Raman spectrometers must have effective filters to keep out Rayleigh scattered radiation while simultaneously recording much weaker Raman scattered radiation. The laser excitation source can be UV, near IR or visible source. If a visible laser is used for excitation, the Raman scattered radiation will also be in the same

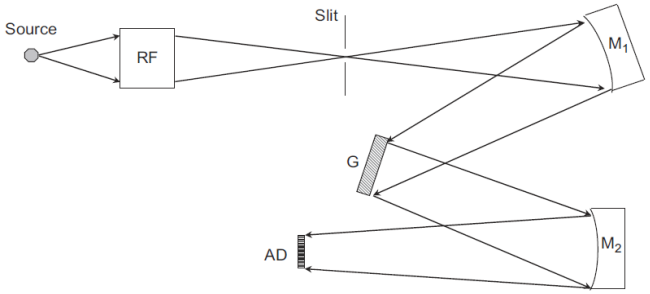

Figure 21: Schematic of a single monochromator Raman spectrometer (89)

range of visible frequencies. A dispersive Raman spectrometer consists of grating which function as individual radiation sources. Incident polychromatic radiation from a laser falls on the gratings and in-phase radiation is incident radiation is reflected onto the exit slit. The radiation is in phase only for select wavelengths where constructive interference takes place. In the other case, when destructive interference takes place, corresponding radiation does not leave the monochromator. The use of effective Rayleigh filters has allowed the utilization of one grating improving optical throughput.

Acquiring spectral information is a trade off between higher throughput and higher resolution. Detectors commonly used include charge-couple-devices (CCD) or array detectors. A schematic of a Raman spectrometer is found in Figure 21 where RF is a Rayleigh filter, G is the grating and M1 and M2 are spherical mirrors and AD is an array detector.

CHAPTER 3

EXPERIMENTAL

3.1 Reagents

- Tin(IV) chloride pentahydrate $SnCl_4.5H_2O$ [Molecular weight 350.6, CAS No. 10026-06-9, Sigma-Aldrich]
- Chromium (III) chloride hexahydrate $CrCl_3.6H_2O$ [Molecular weight: 266.45 g/mole, CAS No. 10060-12-5, Sigma Aldrich]
- Aluminum Chloride hexahydrate $AlCl_3.6H_2O$ [Molecular weight: 241.43 g/mole, CAS No. 7784-13-6, Sigma Aldrich]
- Glucose (Dextrose, D(+)Glucose) $C_6H_{12}O_6$ [Molecular Weight: 180.16 g/mole , CAS No. 50-99-7, Sigma Aldrich]
- Sulfuric acid (volumetric 5 M) H_2SO_4 [Molecular weight: 98.08 g/mole , CAS No. 7664-93-9, Fluka Analytical]
- Hydrochloric acid 36% w/w aqueous solution [Molecular weight: 36.46 g/mole, CAS No. 7647-01-0, Alfa Aesar]

3.2 Preparation of reaction mixtures

1) 1.6 M glucose solutions were prepared in water. 20 mM, 100 mM, 200 mM solutions of metal salts were prepared in water. The solutions were mixed such that final concentrations of 0.8 M glucose in 10 mM, 50 mM and 100 mM metal salt solutions were prepared.
2) 1.6 M glucose solutions were prepared and allowed to equilibrate at room temperature with stirring for 5 hours. These solutions were used to prepare 0.8M glucose solutions in 10mM, 25 mM and 250 mM $AlCl_3$ solutions.
3) 0.8 M glucose solutions were prepared in 0.1 M, 0.05 M and 0.01 M HCl and H_2SO_4 solutions by dissolving 1.6 M glucose solutions in 0.2 M, 0.1 M and 0.02 M HCl and H_2SO_4 solutions respectively.

In all the above cases, once reaction mixtures were prepared, spectral acquisition was carried out every fifteen minutes for 4 hours.

3.3 Spectroscopy

3.3.1 Raman Spectrometer

Raman spectra were recorded using Horiba LabRAM HR Evolution spectrometer. It is a high spatial and spectral resolution Raman spectrometer (UV compatible) equipped with a confocal microscope. It contains air cooled open electrode 1024x256 pixels CCD -75°C and a laser source of 532nm. The additional feature is the UV-Vis-NIR macro lens of 40 mm focal length for open geometry Raman configuration. The spectra were recorded in

dark room to avoid interference of light. Laser-safety goggles were used whenever Raman spectrometer was in use.

Since spectra of liquid samples are to be collected, an external sample holder was used. 1 ml borosilicate vials with a cap was used to hold the samples. Spectra was collected every fifteen minutes for four hours.

Figure 22: Horiba LabRAM HR evolution spectrometer

Figure 23: External arm used for analysis of liquid samples using Raman spectrometer

Acquisition Time: Acquisition time is the actual time over which Raman scattered radiations are counted.

Accumulation Number: The number of distinct acquisition times over which spectra is averaged.

Spectro: If spectrum is collected using spectro, this value is the midpoint of the spectrum obtaiuned.

Parameters	Value
Acquisition time	50 seconds
Accumulations	12
Spectro	1050 cm^{-1}
Laser Intensity	100%
Grating	600 /mm

Table 3: Parameters for Raman spectroscopy

3.3.2 FTIR Spectrometer

FTIR spectra were collected using NICOLET IS50 FT-IR spectrometer. This analytical instrument is a high resolution (~0.9 cm-1) infrared spectrometer and is equipped with DLaTGS and MCT-A detectors. It contains long lifetime Polaris™ infrared source and gold optics. The FTIR is connected to a Parker-Balston 75-45 purge unit to provide a

purified purge gas and air bearing gas from compressed air. The purge gas generator supplies carbon dioxide free air. This helps in obtaining cleaner background spectra in a shorter period of time and more accurate analysis by improving the signal-to-noise ratio. Attenuated Total Reflectance technology is incorporated with this FTIR.

Figure 24: Nicolet FTIR-ATR

Specac ATR is a high-performance single reflection monolithic diamond ATR. One of the characteristic features of this equipment is that it can analyze a wide range of materials irrespective of the material's abrasiveness, hardness, reactivity or corrosiveness. The ATR platform is connected with an electrical heating unit which enables the platform to reach a maximum temperature of 300°C. For the analysis of liquid samples using FTIR-ATR, place a drop of the mixture on the diamond crystal and use the cover slip to prevent surface evaporation during analysis.

Parameters used:

Parameters	Values
Detector	DTGS
Beam Splitter	KBr
Resolution	4 cm^{-1}
Wavenumber range	400-4000 cm^{-1}
Aperture	100
No.of scans	32
Optical Velocity	0.3165 cm/sec

Table 4: Parameters used for ATR-IR spectroscopy

3.4 Normalization of spectra

Mathematical handling of spectroscopic data is highly subjective and dependent on the dataset as well as the type of analysis being targeted- i.e. whether peaks within a spectrum are being compared or whether two different spectra are being compared. Common normalizing techniques include:

1. Division of entire spectrum by intensity of single peak
2. Normalizing over the entire range from 0 to 1 with the formula:

$$Y = \frac{(y_{max} - y)}{(y_{max} - y_{min})}$$

3. Divide the entire spectrum by the area under the spectrum.

In this study, area normalization is followed. The IR spectra is normalized over the region 850-1500 cm^{-1} and for the Raman spectra, the whole range is used. The importance of normalization especially when comparing different samples, consider figures 25 and 26.

In Figure 25, a comparison is made between raw data and normalized data. In the case of

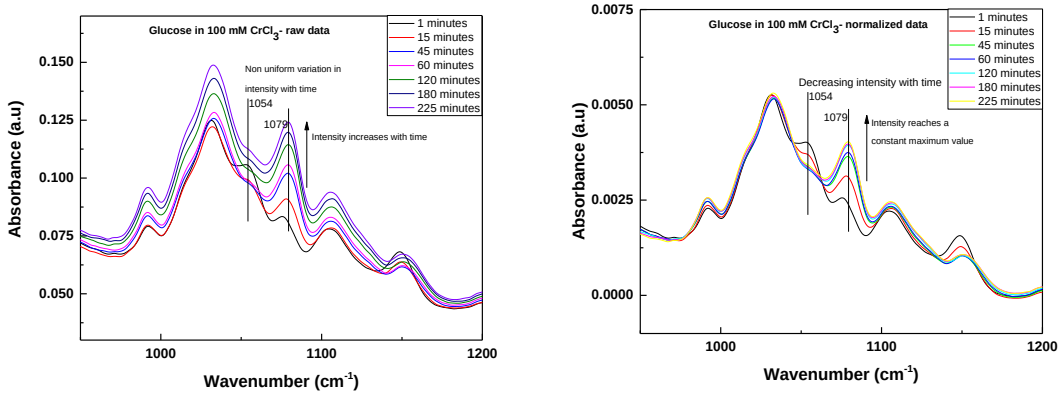

Figure 25: Raw data vs normalized data from IR spectra

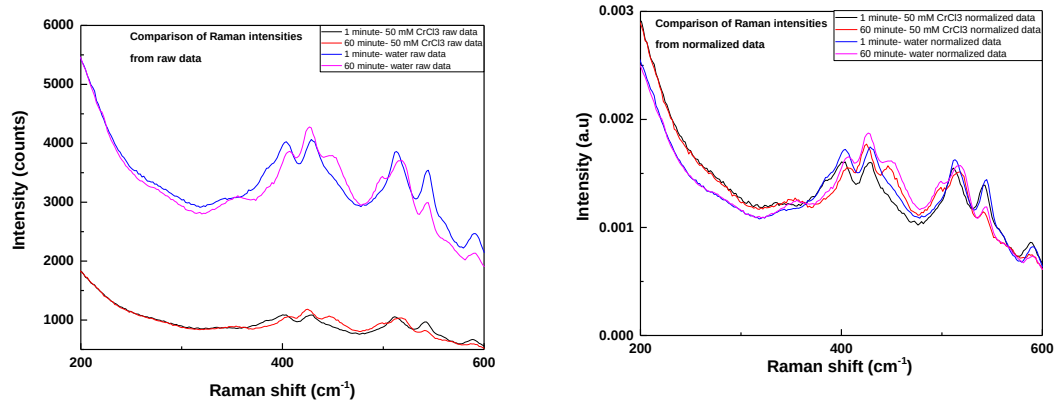

Figure 26: Raw data vs normalized data from Raman spectra

raw data, the variation in peak intensity for the peak at 1054 cm^{-1} does not vary uniformly with time. Additionally, the intensity of peak at 1079 cm^{-1} increases with time indefinitely. In contrast to this, when normalized data is used, the variation in the peak intensity at 1054 cm^{-1} is decreases with time and becomes constant after a certain time. Moreover, the peak at 1080 cm^{-1} increases in intensity with time and eventually reaching a constant value. The information obtained from normalized data allows for determination of equilibrium times. Moreover, knowing that the absorbance is a measure of concentration, the peak at 1057 cm^{-1} and 1080 cm^{-1} cannot increase or decrease indefinitely with time. In the case of raw data, the increase in intensity of a particular vibrational mode is a consequence of an increase in area of the spectrum. In figure 26,comparing the raw values of intensities from 50 mM $CrCl_3$ and water , there is a vast difference in the intensity of Raman scattered radiation. This makes any direct comparison futile. This difference in intensity can be attributed to differences in scattering volume and absorption of radiation by solution. This can be overcome by taking into account the same absorption volume- i.e., normalizing with respect to area of the spectrum. The scales are comparable after normalization. Hence, all data presented in the following section will be from normalized spectra.

CHAPTER 4

RESULTS

4.1 Bands of glucose

Assignments of vibrational modes were made from literature. Several discrepancies were found among assigned vibrational modes. Over fifteen publications were cross checked and tables 5 and 6 summarize the assignments for vibrational modes of glucose obtained from Raman and IR spectroscopy respectively.

Assignments for Raman bands (65) (66) (67) (68) (69) (70) (71) (72) (73) (74):

Raman shift	Vibrational assignment
1625	(HOH) bending mode
1455	(CH2) bending mode
1360	(CH2) wagging mode of beta anomer
1327	(CH2) wagging mode of alpha anomer
1258	(CH2) torsion mode
1120	(COH) bending mode
1080	(C1-O1) stretching mode of beta anomer
1060	(C1-O1) stretching mode of alpha anomer
910	(C1-H1) stretching mode of beta anomer
890	(C1-C2) stretching mode of beta anomer
860	(C1-H1) stretching mode of alpha anomer
842	(C1-C2) stretching mode of alpha anomer
770	(C5-C1-O1) bending mode of beta anomer
710	(O5-C1-O1) bending mode of alpha anomer
585	(C6-C5-O5) bending mode
540	(C2-C1-O1) bending mode of alpha anomer
518	(C2-C1-O1) bending mode of beta anomer
450	Endocyclic (CCO) bending mode
424	(CCC) bending mode
355	(COC) bending mode

Table 5: Assignments for vibrational modes obtained from Raman spectroscopy

Assignments for IR bands (66) (65) (68) (69) (70) (75) (72) (73) (74) (76) (77) (78):

Wavenumber (cm^{-1})	**Vibrational assignment**
1422	(CH_2) scissoring mode
1333	(CH_2) wagging mode
1273	(CH_2) twisting mode
1203	(CH_2) twisting mode
1150	(CO) and (CC) stretching mode
1121	(CC) and (CO) stretching mode and (COH) in plane bending mode
1080	(C1-OH) stretching mode of beta anomer
1060	(C1-OH) stretching mode of alpha anomer
1032	(CC) and (CO) stretching mode and (COH) in plane bending mode
1001	(CCH) and (CCO) in plane bending
915	(CCH) and (CCO) in plane bending
844	(CC) stretching mode

Table 6: Assignments for vibrational modes obtained from IR spectroscopy

Figures 27 and 28 summarize the IR and Raman spectra obtained for glucose in water. The peak positions in water were used as reference for comparing samples with glucose in Lewis acid. From figure 27, it can be observed that the peak at 1054 cm^{-1} decreases in intensity with time while the peak at 1076 cm^{-1} increases in intensity with time. The two peaks are assigned to the (C1-OH) stretching mode of the alpha and beta anomer respectively. It should be kept in mind that hydrogen bonding via glucose-water and

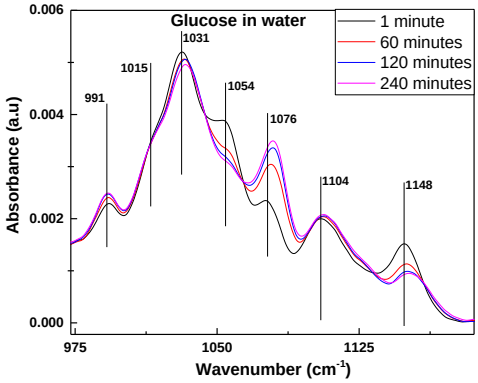

Figure 27: IR spectra of glucose in water

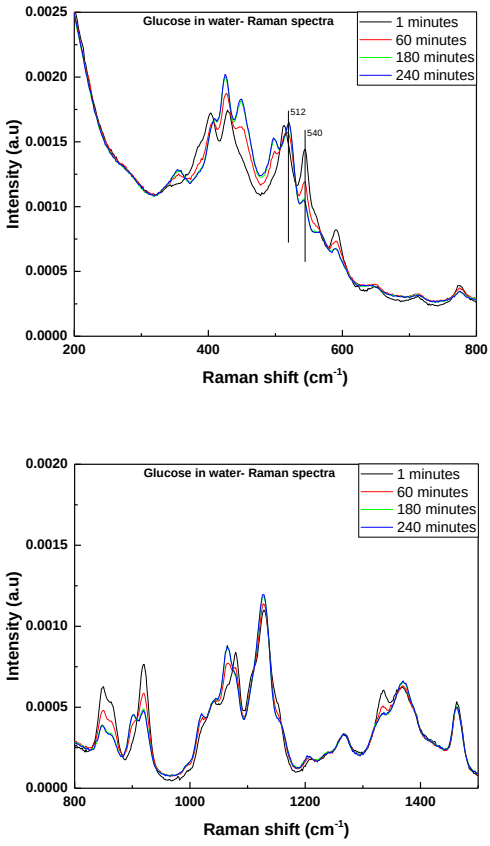

Figure 28: Raman spectra of glucose in water

glucose-glucose interactions exists and thus the peak positions are affected by this. Any significant variation in nature of bonding would lead to red or blue shifts depending on the comparative strength of new bonds with respect to original interactions. The variation in intensity of the (C1-OH) stretching mode of beta anomer with respect to time is studied in greater detail in the following section to comment on the formation of beta-D-glucose. Moreover, the ratio of the peaks at 1054 cm^{-1} and 1076 cm^{-1} is used for the determination of percentages of anomers in solution. Figure 28 displays the Raman spectra of glucose in water. The ratio of intensities of peaks at 512 cm^{-1} and 540 cm^{-1}, the (C2-C1-O1) bending mode of alpha and beta anomers respectively, are used for determination of relative percentage of anomers in solution. The peak at 890 cm^{-1}, which corresponds to C1-C2 stretching mode, is used from the Raman spectra to study the formation of the beta anomer. Therefore, once assignments are made, analysis of peak position as well as the variation in intensity is studied in greater detail in the following sections.

4.2 In-situ Raman and IR spectroscopy of mutarotation

The peak at 1076 cm^{-1} is of interest from the IR spectra and the variation in its intensity is plotted as a function of time in Figure 29. This peak, assigned to (C1-OH) stretching mode of the beta anomer and this is used to track the relative amount of the anomer in solution. This is of significance because the variation in this peak can be used to compare the rate of formation of beta anomer in different Lewis acids. The rate of formation of beta anomer in the presence of $AlCl_3$ is the same as water whereas this rate is faster in the presence of $CrCl_3$ and $SnCl_4$. Moreover, the rate increases as concentration of $CrCl_3$ increases. The time taken to reach equilibrium is summarized in Table 7. It is apparent that the time to reach equilibrium is not uniform as a function of Lewis acid concentration. It is unclear if this is a consequence of the metal atoms present and this variation is probed in the absence of metal salts using Brönsted acids in later sections. Similar information can be obtained from Raman spectrum. Figure 31 shows variation in (C1-C2) stretching mode as a function of time in the presence of Lewis acids. It is clear that the rate of mutarotation is not greatly altered as a function of $AlCl_3$.

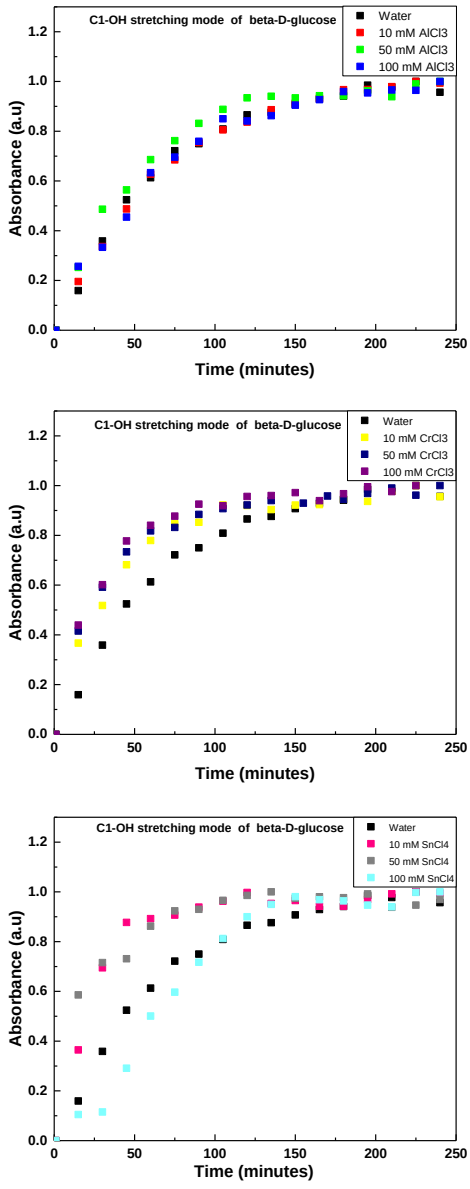

Figure 29: Variation in (C1-OH) Stretching mode from IR spectra

However the rate of mutarotation is faster in $CrCl_3$ and $SnCl_4$ compared to water. Changing concentration of $CrCl_3$ does not produce any change in the rate of formation of beta anomer. However, rate of formation of beta anomer increases as concentration of $SnCl_4$ increases. There is no change in equilibrium time due to concentration of $CrCl_3$.

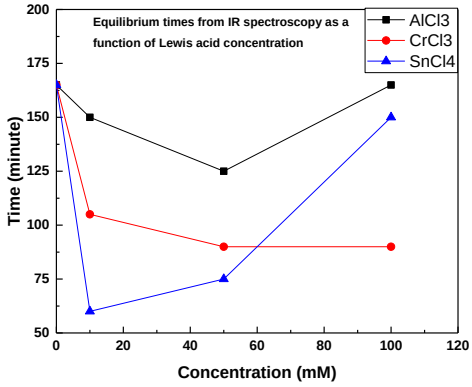

Figure 30: Variation in equilibrium times as a function of Lewis acid from IR spectra

Sample	Time taken to reach equilibrium (min)
Water	165
10 mM $AlCl_3$	150
50 mM $AlCl_3$	125
100 mM $AlCl_3$	165
10 mM $CrCl_3$	105
50 mM $CrCl_3$	90
100 mM $CrCl_3$	90
10 mM $SnCl_4$	60
50 mM $SnCl_4$	75
100 mM $SnCl_4$	150

Table 7: Time taken to reach equilibrium from IR spectroscopy

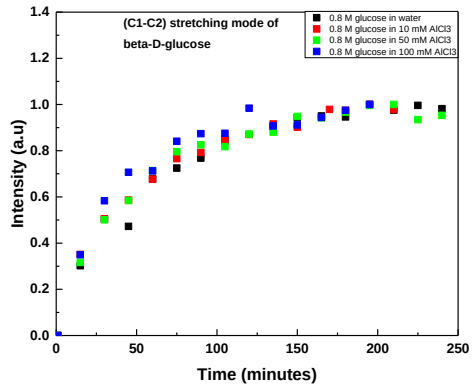

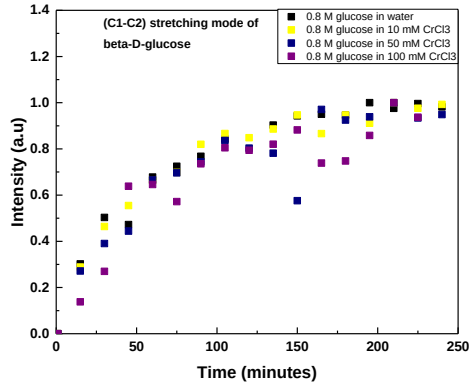

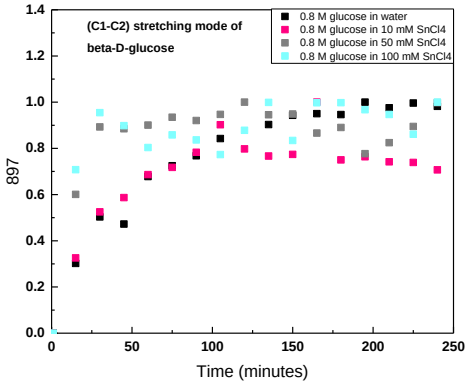

Figure 31: Variation in (C1-C2) stretching mode from Raman spectra

Sample	Time taken to reach equilibrium (min)
Water	150
10 mM $AlCl_3$	90
50 mM $AlCl_3$	125
100 mM $AlCl_3$	165
10 mM $CrCl_3$	90
50 mM $CrCl_3$	90
100 mM $CrCl_3$	90
10 mM $SnCl_4$	75
50 mM $SnCl_4$	60
100 mM $SnCl_4$	30

Table 8: Time taken to reach equilibrium from IR spectroscopy

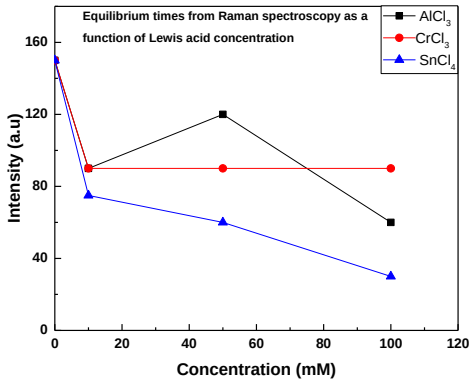

Figure 32: Variation in equilibrium times as a function of Lewis acid from Raman spectra

It is unclear as to why the reaction is fastest in $SnCl_4$. This may be attributed to pH, ionic strength or speciation of metal salts which are individually probed in later sections. It should be noted that this is conflicting with results from IR spectroscopy.

Vibrational modes from IR spectroscopy are littered with interferences and as a consequence overlapping from neighboring vibrational modes. Therefore, results from Raman spectroscopy are used. On the other hand, rather than following the decomposition of alpha anomer or the formation of beta anomer, we can use isosbestic points to determine anomeric pairs and calculate the relative percentage of alpha and beta anomers at equilibrium.

4.3 Effect of Lewis acids and Brönsted acids on equilibrium

Isosbestic points refer to those wavelengths where at least two chemical species have the same molar absorption coefficient which remains constant as reaction proceeds. The presence of an isosbestic point is proof that the stochiometry of a reaction remains unchanged during the reaction. Figure 33 depicts isosbestic points in the 350-600 cm^{-1} range from the Raman spectra. 4 isosbestic points are observed at 408 cm^{-1}, 506 cm^{-1}, 516 cm^{-1}, 530 cm^{-1}. The isosbestic points are preceded and followed by species consumed or

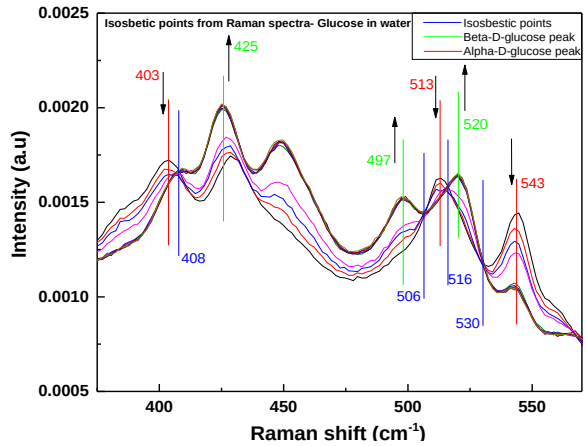

Figure 33: Isosbestic points from Raman spectra

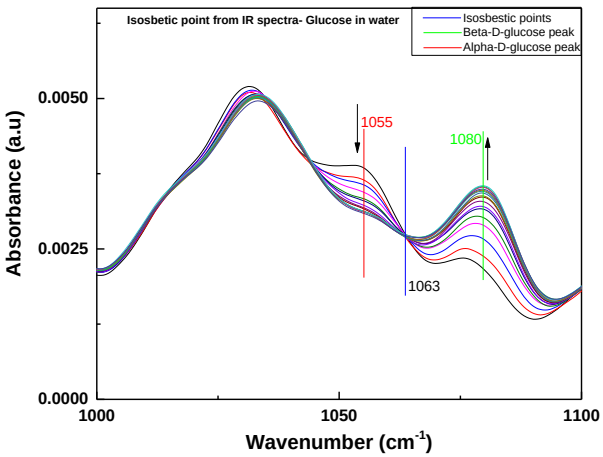

Figure 34: Isosbestic points from IR spectra

formed in reaction. These clearly correspond to the alpha-D-glucose and beta-D-glucose respectively. For the determination of equilibrium percentages, the peaks surrounding the isosbestic point at 530 cm^{-1} are used. Similarly, figure 34 shows the isosbestic point from IR spectra at 1063 cm^{-1}. In both cases, the vibrational assignments are known from literature as follows:

1. 520 cm^{-1}: (C2-C1-O1) bending mode of beta anomer
2. 543 cm^{-1}: (C2-C1-O1) bending mode of alpha anomer
3. 1063 cm^{-1}: (C1-OH) stretching mode of beta anomer
4. 1080 cm^{-1}: (C1-OH) stretching mode of alpha anomer

The equilibrium percentages are calculated as follows:

$$(\%\ alpha - D - glucose)_{Raman} = [I_{543}\ /(I_{543} + I_{520})] \times 100$$

$$(\%\ alpha - D - glucose)_{IR} = [I_{1055}\ /(I_{1055} + I_{1080})] \times 100$$

The calculated equilibrium percentages are compared in Figure 35. Moreover, the relative % alpha anomer is obtained as a function of time from IR and Raman spectroscopy in Figures 36 and 37 respectively.

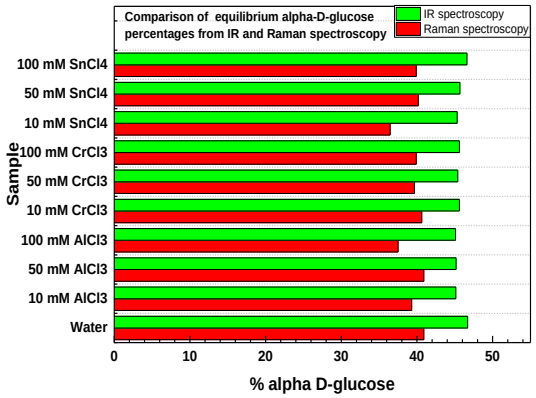

Figure 35: Equilibrium percentages in Lewis acids from IR and Raman spectroscopy

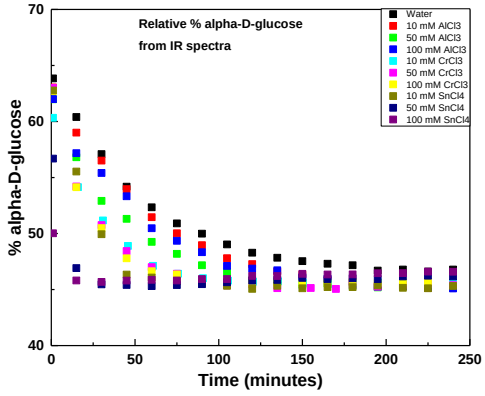

Figure 36: Variation in % alpha-D-glucose in Lewis acids with time from IR spectra

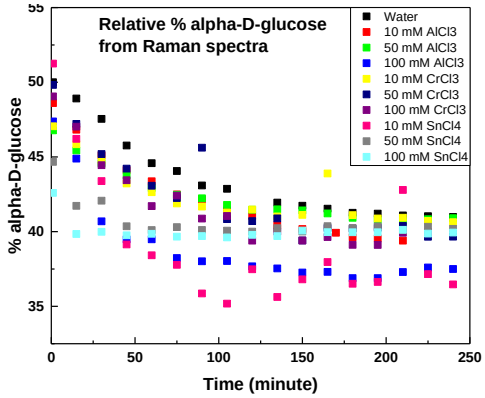

Figure 37: Variation in % alpha-D-glucose in Lewis acids with time from Raman spectra

The final equilibrium percentages (around 39%) from Raman spectroscopy matches more closely with values reported in literature compared to 45% from IR spectroscopy. Moreover, the equilibrium percentages are almost uniform across water and Lewis acids indicating that the presence of Lewis acids has no effect on the equilibrium.

Figures 37 and 38 can be used to compare the rate of mutarotation in Lewis acids. The reaction with $AlCl_3$ is faster than that water. However there appears to be no great difference with change in concentration. It is a similar story for $CrCl_3$ which is almost the same as that in water. However the reaction is fastest in $SnCl_4$ and rate increases with increase in concentration of $SnCl_4$. Therefore in summary, for a given concentration of Lewis acid,

Mutarotation rate: $SnCl_4$>$AlCl_3$>$CrCl_3$> water

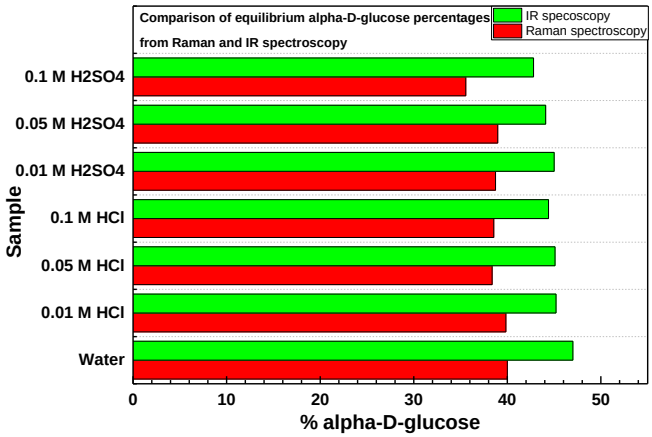

Figure 38: Equilibrium percentages in Bronsted acids from IR and Raman spectroscopy

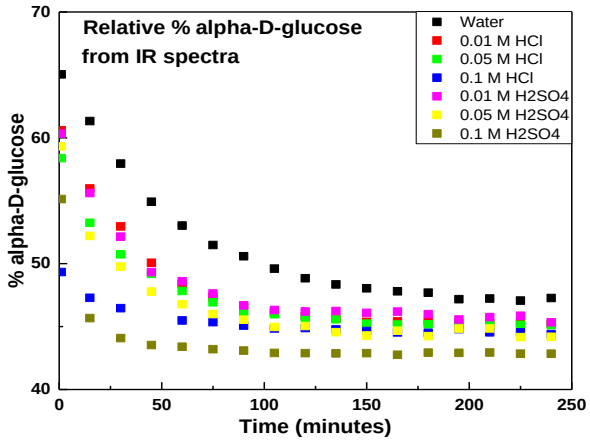

Figure 39: Variation in % alpha-D-glucose in Bronsted acids with time from IR spectra

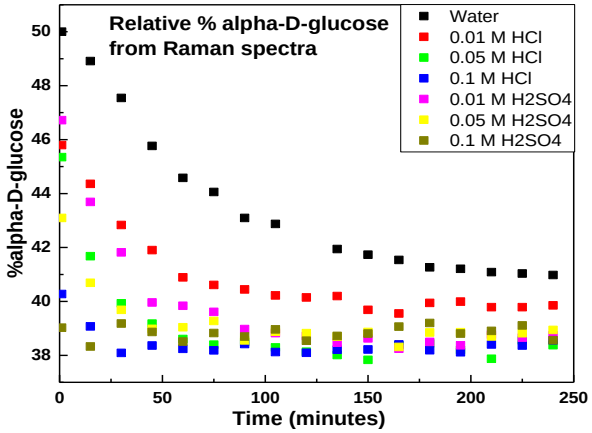

Figure 40: Variation in % alpha-D-glucose in Bronsted acids with time from Raman spectra

Having determined that the presence of Lewis acids alters the rate of mutarotation, it is important to determine the cause of this difference. There are several possible reasons which could explain the variation: presence of metal ions, pH, ionic strength etc.

To analyze the effect of presence of metal salts, mutarotation was studied in the presence of Brönsted acids namely H_2SO_4 and HCl. The relative equilibrium percentages were determined and summarized in Figure 38.

The rate of variation in %alpha-D-glucose was also determined as a function of concentration of the Brönsted acid (Figures 39 and 40).

From figure 38 it is clear that the equilibrium percentage remains fairly constant across concentrations and nature of Brönsted acids used. Analogous to results from Lewis acids, equilibrium percentages

calculated from Raman spectra are better fit to values reported in literature. More significantly, from figures 39 and 40, it is observed that the mutarotation is faster as concentration of acid increases. This is true for H_2SO_4 and HCl. Hence, to summarize mutarotation in Brönsted acids, for a given concentration of acid:

Mutarotation rate: H_2SO_4>HCl> water

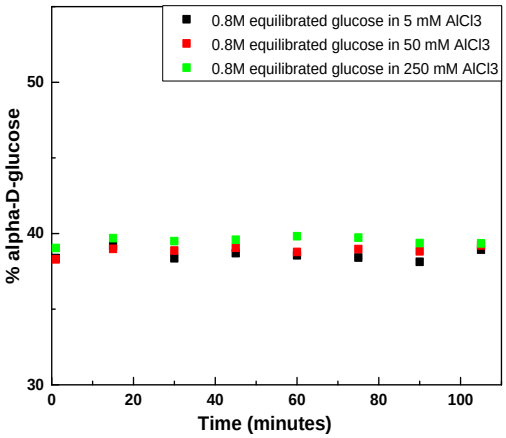

Figure 41: Equilibrated glucose in the presence of $AlCl_3$

To be sure that the equilibrium percentages are independent of the Lewis acid used, another set of experiments were performed. Known concentrations of equilibrated glucose were added to 10 mM, 50 mM and 250 mM $AlCl_3$ and the Raman and spectra was collected. The relative percentage alpha-D-glucose was determined and the results from this experiment are presented in figure 41. It becomes apparent that there is no change in equilibrium as a result of addition of Lewis acid. As a result, we clearly show herein that the presence of homogeneous Lewis acid or Brönsted acid catalyst does not influence the equilibrium of glucose anomers but based on the discussion in previous paragraphs, only the kinetics. This important result can decouple these two effects and provide useful insights into reaction modelling The rate of mutarotation can also be affected by interactions between glucose-metal salts. Metal atoms could bind to the intermediate or to one of the anomeric forms thereby altering the stability. These glucose-metal salt interactions are discussed in the next section.

4.4 Insights into Glucose-Metal salt interactions

Analysis of peak position from IR and Raman spectra provides information on the nature of bonding. It should be kept in mind that hydrogen bonding via glucose-water and glucose-glucose interactions exist and thus the peak positions are affected by this.

Any significant variation in nature of bonding would lead to red or blue shifts depending on the comparative strength of new bonds with respect to original interactions. Figures 42 and 43 shows IR and Raman spectra of glucose in metal salts at 1 min and 240 min respectively. There is no variation in peak position due to the addition of Lewis acid. This indicates the absence of any long time glucose- metal salt interactions. It should be noted that unstable complexes with lifetimes too low to be picked up using spectroscopic techniques cannot be studied using this approach. Moreover, the absence of new peaks

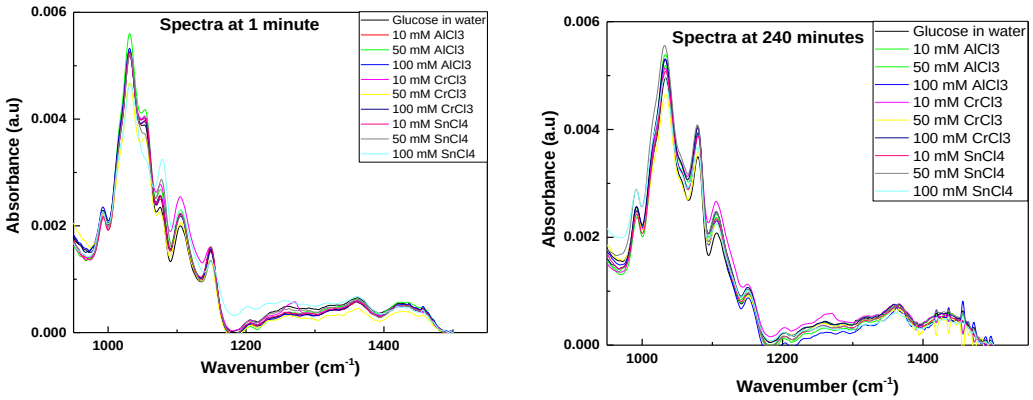

Figure 42: Comparison of peak position from IR spectra

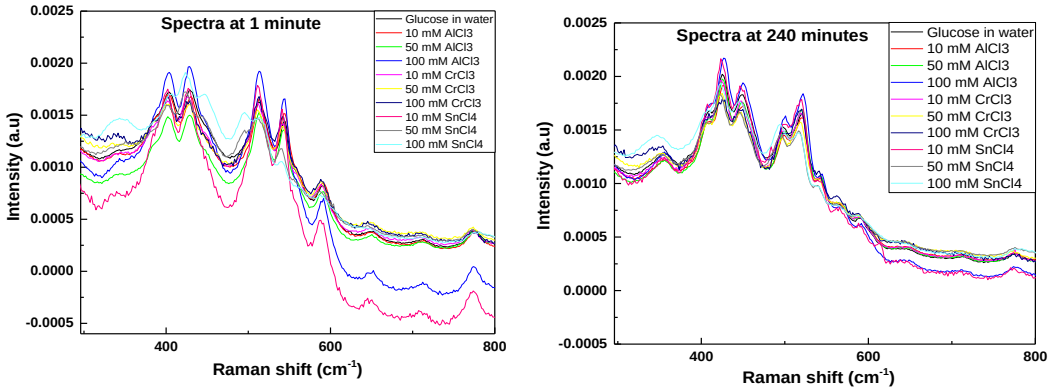

Figure 43: Comparison of peak position from Raman spectra

also highlights the absence of an IR or Raman active intermediate. There appears to be variations in the peak at 350 cm^{-1} in the Raman spectra. However, these variations are less than 5 cm^{-1}. In figure 44, the Raman spectra of Lewis acid in water in shown. Attention must be paid to the peak at 339 cm^{-1} which increases as concentration of metal salt increases. Therefore, the variations in the peak at 350 cm^{-1} can be attributed to interference from the spectra of Lewis acid.

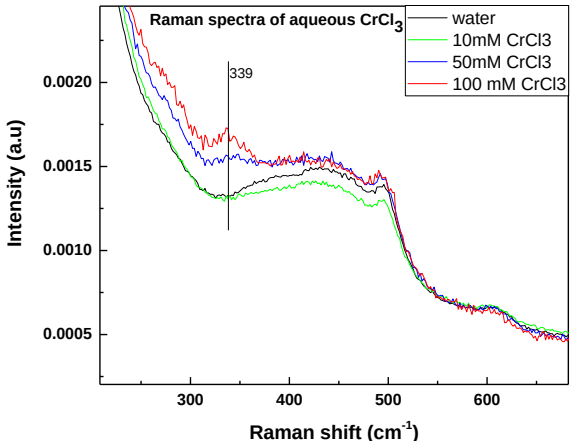

Figure 44: Raman spectra of Lewis acids

To conclude, the presence of metal salts influences rates of mutarotation with no visible long time interactions with glucose molecules.

This result holds true for $AlCl_3$, $CrCl_3$ and $SnCl_4$. However, metal salts can form a plethora of complex species with water and this is discussed in later sections. The glucose-water interactions, on the other hand, can be studied by determining the ratio of intensity between CH_2 scissoring mode and HOH bending mode i.e the ratio obtained from bands at 1420 and 1640 cm^{-1} respectively and monitoring the change in this ratio with time. Reduced glucose-water interactions are depicted by an increase in this ratio (66). Figure 45 indicates that the ratio remains fairly constant as a function of time with the only exceptions being 50 mM $SnCl_4$ and 100 mM $SnCl_4$ in which an increase in this ratio is observed. Additionally, with the exception of the two tin samples, the ratio is lower than water indicating enhanced interactions between glucose and water. There is significant difference for the two tin samples with time indicating strong glucose-water interactions at low times but subsequent weakening of these interactions. This could explain rapid mutarotation in $SnCl_4$ at the start of the reaction. Since metal-salt interactions are still unknown, the next section will focus on the species formed as a result of metal salt-water interactions.

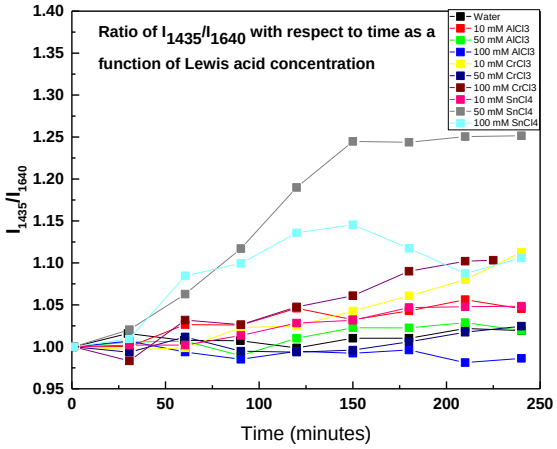

Figure 45: Variation in intensity ratio

4.5 Speciation of metal salts

To study Lewis acid-water interactions, equilibrium speciation software, Minteq is used. Minteq is used to determine the nature and concentration of species formed as a consequence of Lewis acid-water interactions. The concentration of the metal salt (in molal) is the input and the mass and charge balance model is used. This model is based on the premise that *the quantity of all species in a solution containing a particular atom (or a group of atoms) must be equal to the amount (or group) delivered to the solution and that in any solution the sum of positive charges is equal to the sum of negative charges.*

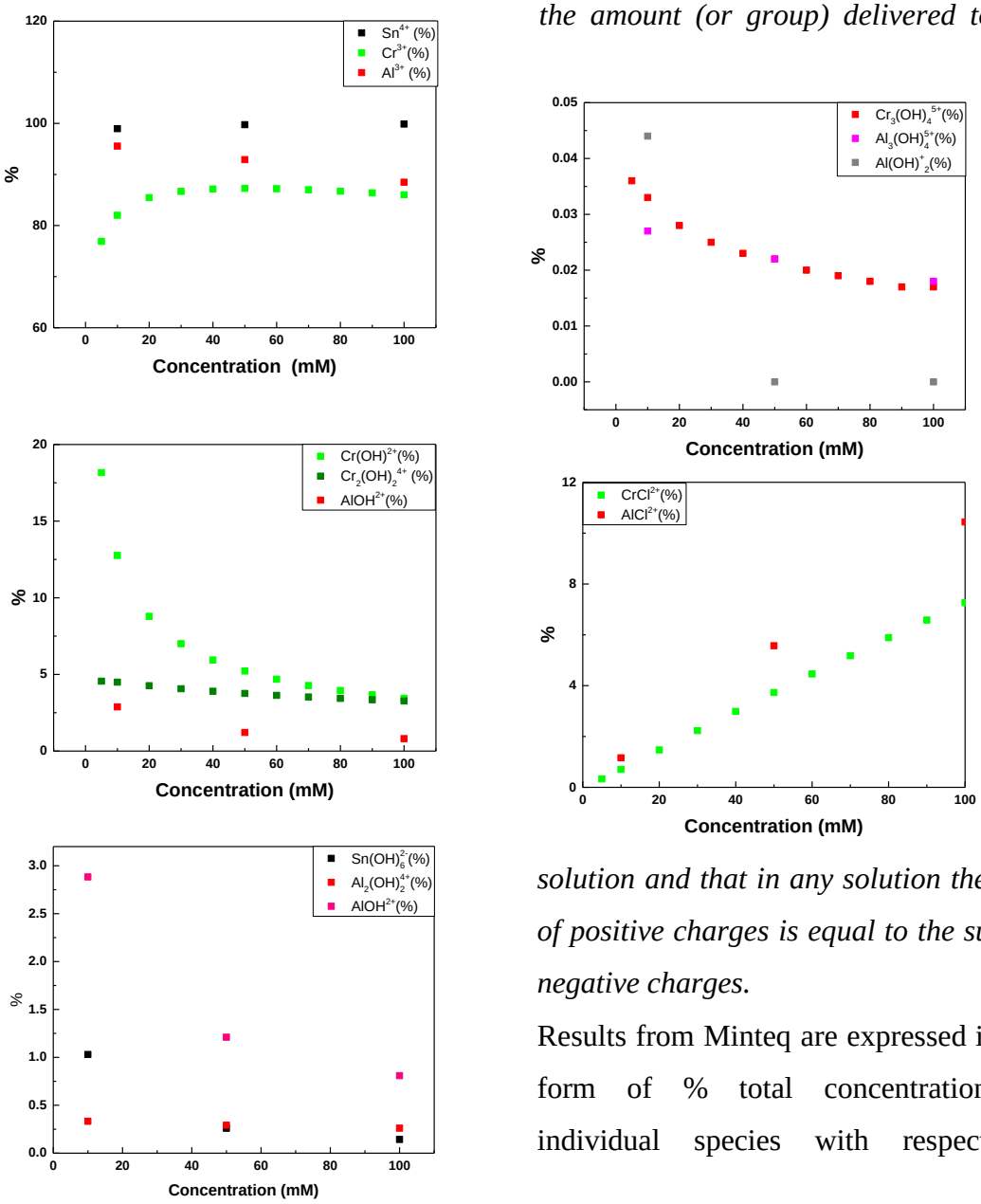

Figure 46: Water-metal salt complexes from MINTEQ

Results from Minteq are expressed in the form of % total concentration of individual species with respect to

concentration of metal salt in figure 46. Minteq utilizes activity coefficients to determine speciation. Therefore, information on speciation is obtained under the condition zero ionic strength. At this condition, the activity of ions is equal to the concentrations as activity coefficient is 1. Simulations fail when run without fixing ionic strength at high concentrations of chromium and tin. Therefore, for uniformity in comparison, the ionic strength is fixed at zero.

Minteq predicts 6 different species of alumium chloride which exist at concentrations of interest- Al^{3+} denotes free aluminum ions in solution, $AlCl^{2+}$ indicates partially undissociated $AlCl_3$ and $Al(OH)_2^{+}$, $AlOH^{2+}$, $Al_2(OH)_2^{4+}$ and $Al_3(OH)_4^{5+}$ indicate aluminum- water complexes. At low concentrations of $AlCl_3$, most of the aluminum ions exist in the free state in solution i.e as Al^{3+} ions. As the concentration of metal salt increases, relative percentage of free Al^{3+} ions decreases. The $Al(OH)_2^{+}$ exists only at low concentrations of salt. Further, increase in concentration of salt also leads to a decrease in the aluminum-water complexes although the rate of decrease is not linear. Although increasing concentration of aluminum salt decreases the free Al^{3+} in solution, this does not lead to an increase in aluminum-water complexes: relative percentages of $AlOH^{2+}$, $Al_2(OH)_2^{4+}$ and $Al_3(OH)_4^{5+}$ decrease with increasing concentration of the aluminum salt and that of $Al(OH)_2^{+}$ becomes zero. This is offset by an increase in $AlCl^{2+}$ is observed. This can be attributed to an increase in salt-salt interactions rather than salt-water interactions.

Variation in chromium chloride speciation with respect to concentration of $CrCl_3$ is also obtained. Minteq predicts 5 different species that exist in this range. Cr^{3+} which is the free chromium in solution, complexes with water $Cr(OH)_2^{4+}$, $Cr_3(OH)_4^{5+}$ as well as $Cr(OH)^{2+}$ in addition to the chloride $CrCl^{2+}$. Increase in concentration of salt leads to an increase in free chromium until a maximum is reached beyond which there is a slight decrease in relative percentage of free chromium. The percentage of complexes with water decreases with increasing concentration of salt which leads to a corresponding increase in the chloride form. This variation is very similar to aluminum.

For tin chloride, minteq predicts only 2 species; free tin species Sn^{4+} and the complex with water $Sn(OH)_6^{2-}$. Interestingly, tin is the only salt capable of forming anions on

complexation with water. This can be attributed to increased electronegativity of tin compared to chromium and aluminum.

One uniform observation from speciation using MINTEQ is that the percentage of $M(OH)_x^{y+}$ species i.e., water-metal complexes decrease as concentration increases. Further, percentage of free cations (metal ions) in solution remains constant for tin, increases with concentration for chromium and decreases as concentration increases for aluminum. On the other hand, the nature of species formed is significantly different for tin compared to aluminum and chromium. Kinetics of mutarotation obtained from earlier sections indicate that the rate of mutarotation reaction increases as the concentration of $SnCl_4$ increases but remains fairly uniform with changes in concentration of $CrCl_3$ and $AlCl_3$.

Results on Brönsted acids however show uniform variations with respect to acid concentration. It is important to know whether increased rates with increased concentrations are a function of pH, ionic strength or a combination of both.

4.6 pH and ionic strength considerations

Since there is no correlation between individual species of metal salts and rate of mutarotation, ionic strengths were calculated to determine if the variatiation in this rate is dependent on the number of ions in solution rather than the nature of ions. Calculated ionic strength in mmoles/litre takes into account concentration and charge of the cation and anion under consideration.

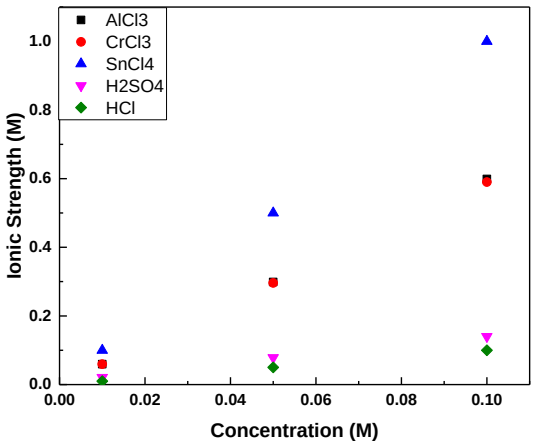

Figure 47: Variation in ionic strength

$$I = \frac{1}{2} \Sigma C_i z_i^2$$

where C_i is the concentration and Z_i is the valency of component i

The ionic strength of $SnCl_4$ is greater than $AlCl_3$ and $CrCl_3$ of the same concentration. Mutarotation was found to be faster in $SnCl_4$ compared to $AlCl_3$ and $CrCl_3$. A reaction can be sped up or slowed down by controlling the ionic strength depending on the

mechanism. This is of great importance especially in cases where in the intermediate formed is between two cations or anions. In this example, reaction can be sped up by increasing ionic strength. On the other hand, an intermediate formed between a cation and an anion is stabilized at higher ionic strengths which would slow down the reaction. Lowry (23) demonstrated the proportional effect of acid and base concentration on the rate of mutarotation. The rate of mutarotation was found to be directly proportional to the square root of acid concentration and directly proportional to the concentration of alkali. This indicates in addition to ionic strength, other factors

Concentration (M)	pH of $AlCl_3$	pH of $CrCl_3$	pH of $SnCl_4$	pH of H_2SO_4	pH of HCl
0.1	2.958	2.172	3.063	1.496	1.01
0.05	3.112	2.347	3.106	1.699	1.387
0.01	3.827	2.762	3.206	2.206	2.045

Table 9: pH of Lewis and Brönsted acids used

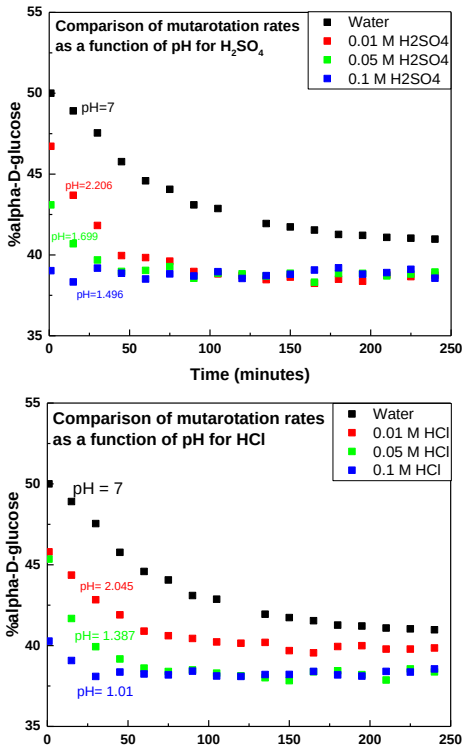

Figure 48: Variation in rates as a function of pH for the same acid

also play a role in the rate kinetics. Lowry further concluded that the mutarotation remains unchecked by neutralization and remains unaffected by acidic or basic impurities. In keeping with these results, the mutarotation of glucose was probed in three concentrations of HCl and H_2SO_4 solutions whose ionic strengths along with those of Lewis acids used are summarized in figure 47.

Further, the ionic strength of metal salts is much higher than acids for the same concentration in water. However, taking into account the lack of metal salt-glucose interactions, the comparison of mutarotation kinetics with respect to pH would be more pertinent. pH takes into

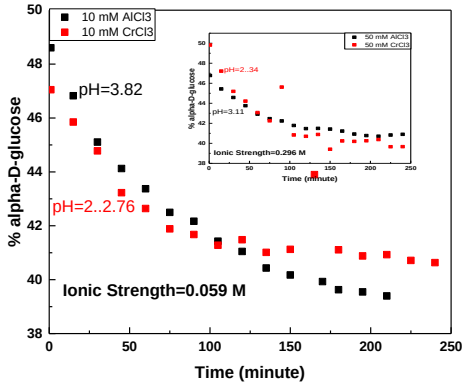

Figure 49: Comparing mutarotation rates for different species at same ionic strength

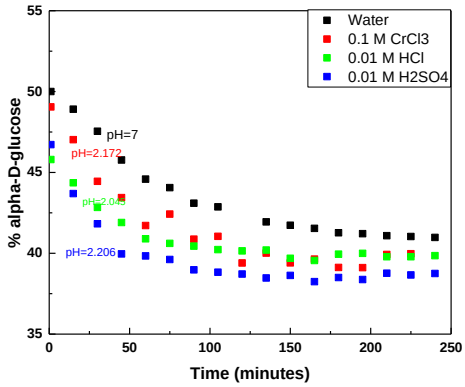

Figure 50: Variation in rates as a function of pH for 3 different acids

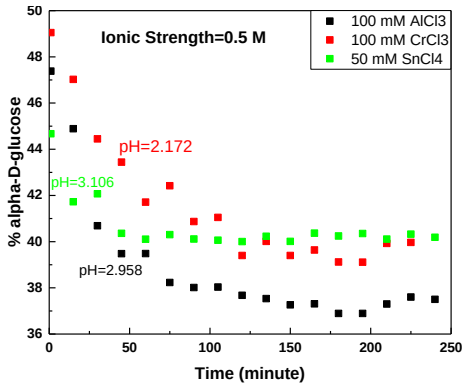

Figure 51: Comparison of mutarotation rates at higher ionic strength

consideration only the free hydrogen ions in solution in contrast to ionic strength which takes into account all ions and their valencies. Table 9 indicates the pH of acids and metal salts used in this study.

Comparing rate of mutarotation for systems consisting of the same species (Figure 48), rate increases with lower values of pH and increasing values of ionic strength for Brönsted acids. This is indication that when the solution contains no metal ions, there exists monotonic variation in rate with respect to the acid concentration. This is further indication that the nature of metal-water species formed despite not bonding to glucose contribute to the kinetics. The same variation does not hold true for high ionic strength. $AlCl_3$ and $CrCl_3$ have the same ionic strength but different pH values. Figure 49 shows that at constant ionic strength, the mutarotation rates are identical.

Figure 50 compares the rate of mutarotation in 0.01 M H_2SO_4, 0.01 M HCl and 0.1 M $CrCl_3$: 3 solutions of comparable pH and water. From this figure, it is clear that the mutarotation reaction is faster in solutions whose pH is lower than that of water. On the other hand, this consumption rate is not a linear function of the pH when different species are involved as. The mutarotation is fastest in 0.01 M H_2SO_4 despite this solution

having a higher pH than 0.01 HCl and 0.1 M $CrCl_3$. On the other hand ionic strength varies as follows for the acids compared: $CrCl_3$>H_2SO_4> HCl but mutarotation is fastest in H_2SO_4.

In conclusion, for Brönsted acids, the rate of mutarotation increases as acid strength (lower pH and higher ionic strength) increases. In the case of Lewis acids, at low ionic strengths, mutarotation rates are identical for different species. However, this fails when different species exist in solution (figure 51). This may also be attributed to differences in electronegativity between Al (1.61) and Cr (1.66) becoming more significant at higher concentrations.

CHAPTER 5

CONCLUSIONS

It has been shown that vibrational spectroscopy is a very capable tool for the in-situ study of mutarotation in glucose in homogeneous catalysts. Compared to IR spectroscopy, Raman spectroscopy is a superior tool for analysis of such systems due to less interference from neighboring bands. Results from IR and Raman spectra indicate that there is no interaction between glucose and metal salts. However, the presence of metal salts, namely $CrCl_3$, $AlCl_3$ and $SnCl_4$ aid the mutarotation reaction leading to formation of beta-D-glucose from alpha-D-glucose. The relative equilibrium percentages of alpha-D-glucose and beta-D-glucose obtained from Raman spectra match well with values reported in literature (36%-64% respectively).

Rate of mutarotation is fastest in $SnCl_4$ wherein the rate increases with concentration of $SnCl_4$. The rate of mutarotation does not vary significantly with concentration of $AlCl_3$ and $CrCl_3$ but in both cases the reaction is faster than in water. Differences in nature of glucose-water interactions from ratio of intensities of CH_2 bending mode to OH bending mode of water with time for tin chloride might offer an explanation for increased mutarotation rates wherein glucose-water interactions are strong initially but become weaker with time. Since glucose-metal salt interactions were not visible from spectroscopy but the presence of the metal salt alters the rate of mutarotation, it can be concluded that the presence of metal salt has a significant effect on glucose-water and water-water interactions. Although increasing ionic strength leads to faster mutarotation for $SnCl_4$, a similar observation is not seen for aluminum and chromium chloride. In order to further highlight the influence of metal atoms in solution, mutarotation was studied in Brönsted acids. In the case of Brönsted acids, there is uniform variation with respect to ionic strength. Increasing acid concentrations led to faster mutarotation rates for Brönsted acids. It has been shown that water-water interactions can be substituted by glucose-water interactions (79). This leads to an increase in hydrogen bonding in a glucose-water system compared to a system containing pure water since the number of water molecules that can bond to a glucose molecule ranges from 4 to 9. A decrease in the highly reactive OH groups of water on addition of glucose has been reported (79). On the other hand, Minteq studies have shown that the nature of species formed is significantly different for Sn compared to Al and Cr which could contribute to

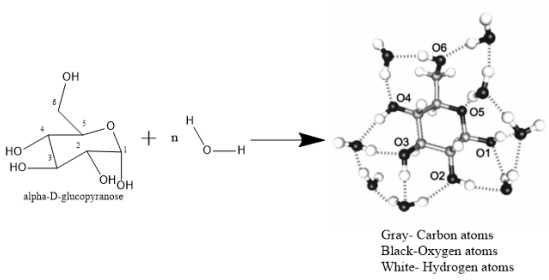

Figure 52: Structure of Glucose-water complex with 8 water molecules (80)

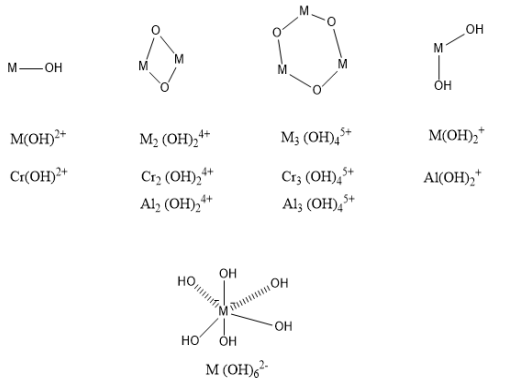

Figure 53: Structure of Metal salt water complexes (102)

faster mutarotation rates and in all cases, metal species are formed with varying number (OH) groups. The tendency of metal salts to form such species leads to breaking of water-glucose bonds thereby influencing the mutarotation reaction.

Glucose-water complexes with 8 or 9 molecules of water bonded to glucose were studied (80). Addition of metal salts to glucose-water systems causes variations in this bonded network by metal salts combining with the highly reactive OH groups of water.

The mutarotation which is carried out by protonation is aided by metal salts combining with OH groups of water. The greater the number of OH groups of water molecules a metal salt is capable of binding with, faster is the mutarotation rate. This could offer an explanation as to why the reaction is fastest in $SnCl_4$ and remains fairly uniform in $CrCl_3$ and $AlCl_3$ and faster than water. The variation in rate of mutarotation is uniform with respect to concentration of Brönsted acids due to uniform increase in protons in solution.

Although this work addresses rate of mutarotation in Lewis acids, no information on possible short lived interactions between glucose and metal salt were obtained. More metal salts can be studied to determine if there is a definitive variation in mutarotation rates with respect to the number of OH groups to which the metal salt can bind with. This would also enable the determination of generic equations that describe variations in mutarotation rates depending on position of a metal cation in the periodic table. Once effects of Lewis acids on mutarotation rates are known and the impact of acidity understood, solid catalysts with desired structures and Lewis acidities can be used in

place of liquid catalysts. This reaction can also be studied at lower temperatures as this would slow down mutarotation rates making it easier for analysis. The speciation of metal salts varies with temperature and hence the effect of temperature on mutarotation rates can also be studied in greater detail as a function of the metal salt. This work remains a frontrunner in the study of homogeneous Lewis acid catalyzed mutarotation using vibrational spectroscopy. Several pertinent questions still remain unanswered which makes the study of this system vital if the dream of the biorefinery concept is ever to be fulfilled.

REFERENCES

Bibliography

1. *Synergistic Saccharification, and Direct Fermentation to Ethanol, of Amorphous Cellulose by Use of an Engineered Yeast Strain Codisplaying Three Types of Cellulolytic Enzyme.* **Yasuya Fujita, Junji Ito, Mitsuyoshi Ueda, Hideki Fukuda and Akihiko Kondo.** 2, 2004, Applied and Environmental Microbiology, Vol. 70, pp. 1207-1212.

2. *Direct conversion of cellulose/hemicellulose to ethanol by Neurospora crassa.* **Vasanti Deshpande, Sulbha Keskar, Chitra Mishra, Mala Rao.** 3, 1986, Enzyme and Microbial Technology, Vol. 8, pp. 149-152.

3. *Direct fermentation of cellulose to ethanol by a cellulolytic filamentous fungus, Monilia sp.* **Tsao, Cheng-shung GongChristine M. MaunGeorge T.** 2, 1981, Biotechnology Letters, Vol. 3, pp. 77-82.

4. *Enhanced Cellulose Fermentation by an Asporogenous and Ethanol-Tolerant Mutant of Clostridium thermocellum.* **P. Tailliez, H.Girard, J. Millet and P. Beguin.** 1, 1989, Applied and Environmental Microbiology, Vol. 55, pp. 207-211.

5. *Lignin pyrolysis products, lignans, and resin acids as specific tracers of plant classes in emissions from biomass combustion.* **Bernd R. T. Simoneit, W. F. Rogge, M. A. Mazurek, L. J. Standley, L. M. Hildemann, G. R. Cass.** 12, 1993, Environmental Science and Technology, Vol. 27, pp. 2533-2541.

6. *Gasification of Cellulose, Xylan, and Lignin Mixtures in Supercritical Water.* **Matsumura, Takuya Yoshida and Yukihiko.** 23, 2001, Industrial and Engineering Chemistry Research, Vol. 40, pp. 5469-5474.

7. *The emerging role for bacteria in lignin degradation and bio-product formation.* **Timothy DH Bugg, Mark Ahmad, Elizabeth M Hardiman, Rahul Singh.** 3, June 2011, Current Opinion in Biotechnology, Vol. 22, pp. 394-400.

8. *Ubiquitous aluminum alkyls and alkoxides as effective catalysts for glucose to HMF conversion in ionic liquids.* **Dajiang (DJ) Liu, Eugene Y-X. Chen.** 2012, Applied Catalysis A: General, Vols. 435-36, pp. 78-85.

9. *Efficient conversion of glucose into 5-hydroxymethylfurfural catalyzed by a common Lewis acid SnCl4 in an ionic liquid.* **Suqin Hu, Zhaofu Zhang, Jinliang Song, Yinxi Zhoua and Buxing Han.** 11, 2009, Green Chemistry, pp. 1746-1749.

10. *Direct conversion of glucose and cellulose to 5-hydroxymethylfurfural in ionic liquid under microwave irradiation.* **Changzhi Lia, Zehui Zhanga, Zongbao K. Zhao.** 38, 2009, Tetrahedron Letters, Vol. 50, pp. 5403-5405.

11. *Biomass recalcitrance: engineering plants and enzymes for biomass production.* **Himmel ME, Ding SY, Johnson DK, Adney WS, Nimlos MR, Brady JW, Foust TD.** 2007, Science, Vol. 315, pp. 804-807.

12. *Molecular and industrial aspects of glucose isomerase.* **S H Bhosale, M B Rao, and V V Deshpande.** 2, 1 June 1996, Microbiology and Molecular Biology Reviews, Vol. 60, pp. 280-300.

13. *Mechanism of Glucose Isomerization Using a Solid Lewis Acid Catalyst in Water.* **Yuriy Román-Leshkov, Manuel Moliner, Jay A. Labinger, Mark E.Davis.** 47, 2010, Angewandte Chemie, Vol. 49, pp. 8954-8957.

14. *Mechanistic Insights into Lewis Acid Metal Salt-Catalyzed Glucose Chemistry in Aqueous Solution.* **Hannah Nguyen, Vladimiros Nikolakis, and Dionisios G. Vlachos.** 3, 2016, ACS Catalysis, Vol. 6, pp. 1497-1504.

15. *"One-Pot" Synthesis of 5-(Hydroxymethyl)furfural from Carbohydrates using Tin-Beta Zeolite.* **Eranda Nikolla, Yuriy Román-Leshkov, Manuel Moliner, and Mark E. Davis.** 4, 2011, ACS Catalysis, Vol. 1, pp. 408-410.

16. *Metal Chlorides in Ionic Liquid Solvents Convert Sugars to 5-Hydroxymethylfurfural.* **Haibo Zhao, Johnathan E. Holladay, Heather Brown, Z. Conrad Zhang.** 5831, 2007, Science, Vol. 316, pp. 1597-1600.

17. *Kinetics of glucose isomerization to fructose by immobilized glucose isomerase: anomeric reactivity of d-glucose in kinetic model.* **Han Seung Lee, Juan Hong.** 2, 2000, Journal of Biotechnology, Vol. 84, pp. 145-153.

18. *Mechanistic Study of Glucose-to-Fructose Isomerization in Water Catalyzed by [Al(OH)2]+.* **Jinqiang Tang, Xiawei Guo, Liangfang Zhu,and Changwei Hu.** 2015, Vol. 5, pp. 5097-5103.

19. *Studies on the forms of d-glucose and their mutarotation.* **C. S. Hudson, J. K. Dale.** 2, 1917, J. Am. Chem. Soc, Vol. 39, pp. 320-328.

20. **D. Rittenberg, C. Graff.** 1956, J. Am. Chem. Soc, Vol. 80, pp. 3370-3372.

21. *The reduction of aldoses at the dropping mercury cathode: Estimation of the aldehydo structure in aqueous solutions.* **S.M. Cantor, Q.P. Peniston.** 8, 1940, J. Am. Chem. So, Vol. 62, pp. 2113-2121.

22. *The Kinetics of Mutarotation of D-Glucose with Consideration of an Intermediate Free-aldehyde Form.* **J. M. Los, L. B. Simpson, K. Wiesner.** 8, 1956, Vol. 78, pp. 1564-1568.

23. *T.Martin Lowry, D.Sc.* **glucose, Studies of Dynamic Isomerism. I. The mutarotation of.** 1903, Journal of Chemical Society, Transactions , Vol. 83, pp. 1314-1323.

24. *Mutarotation of Sugars in solution: Part 1: History, Basic Kineticsand Composition of Sugar Solutions.* **Pigman W, Isbell H.** 1968, Advanced Carbohydrate Chemistry, Vol. 23, pp. 11-57.

25. *The Kinetics of the mutarotation of glucose, catalyzed by hydrogen ion in aqueous solution.* **P.Johnson, E.A.Moelwyn-Hughes and.** 1941, Transactions of the Faraday Society, Vol. 37, pp. 289-292.

26. *Kinetic Parameters for the noncatalyzed and Enzyme-Catalyzed Mutarotation of Glucose using a blood Glaucometer.* **John R hardee, Bryan Delgado and Wray Jones.** 2011, Journal of Chemical Education, Vol. 88, pp. 798-800.

27. *The mutarotation of glucose in frozen aqueous solutions.* **Pincock, Thomas E Kiovsky and Richard E.** 20, 1966, Journal of American Chemical Society, Vol. 88, pp. 4704-4710.

28. *The mutarotation of glucose in water-methanol mixtures_Acetate Ion Catalysis.* **Thumm, Douglas G Hill and Byron A.** 6, 1952, J. Am. Chem. Soc, Vol. 74, pp. 1380-1382.

29. *Base catalyzed mutarotation of glucose in dimethylformamide and dimethyl sulfoxide.* **Brian G Cox, Rajagopalan natarajan.** 1977, Jounal of Chemical Society, Perkin Transactions 2, Vol. 0, pp. 2021-2024.

30. *Theoretical Study of mutarotation og Glucose.* **Yamabe, Shinichi.** 1999, Journal of Organic Chemistry, Vol. 64, pp. 4519-4524.

31. *Glucose-isomerase-catalyzed D-glucose-D-fructose interconversion: Mechanism and reactive species.* **M.Makkee, A.P.G.Kieboom, H.Van Bekkum.** 12, 1984, Recueil des Travaux Chimiques des Pays-Bas, Vol. 103, pp. 361-364.

32. *Continuous Isomerization of glucose to fructose on a commercial basis.* **B.J.Schnyder.** 1974, Die Starke, Vol. 12, p. 412.

33. *Anomer Specificity during some isomerase reactions.* **Milton S Feather, Vijay Deshpande and Michael J Lybyer.** 5, 1970, Biochemical and Biophysical Research Communications, Vol. 38, pp. 859-863.

34. **Miljkovic, Momcilo.** *Carbohydrates: Synthesis, Mechanisms and Stereoelectronic Effects.* New York : Springer, 2009. 1441909044, 9781441909046.

35. *Enolisation and isomerisation of monosaccharides in aqueous, alkaline solutions.* **G de Wit, A.P.G.Kieboom, H van Bekkum.** 1, 1979, Carbohydrate Research, Vol. 74, pp. 157-175.

36. **Parrish, F W.** *Isomerization of glucose, maltose and lactose with amino compouonds. 3514327A* US, 26 May 1970.

37. *Effect of Borate on the Alkali-catalyzed Isomerization of Sugars.* **Mendicino, Joseph F.** 18, 1960, J. Am. Chem. Soc, Vol. 82, pp. 4975-4979.

38. *Complexes of carbohydrates with aluminate ion. Aldose-ketose interconversion on anion-exchange resin (aluminate and hydroxide forms).* **Jacob A.Rendleman Jr, John E.Hodge.** 1979, Carbohydrate Research, Vol. 75, pp. 83-99.

39. *Kinetic and Mechanistic Study of Glucose Isomerization Using Homogeneous Organic Brønsted Base Catalysts in Water.* **Jack M. Carraher, Chelsea N. Fleitman and Jean-Philippe Tessonnier.** 6, 2015, ACS Catalysis, Vol. 5, pp. 3162-3173.

40. *Mechanistic Study of Glucose-to-Fructose Isomerization in Water Catalyzed by [Al(OH)2(aq)]+.* **Jinqiang Tang, Xiawei Guo, Liangfang Zhu and Changwei Hu.** 9, 2015, ACS Catalysis, Vol. 5, pp. 5097-5103.

41. *Insights into the Interplay of Lewis and Brønsted Acid Catalysts in Glucose and Fructose Conversion to 5-(Hydroxymethyl)furfural and Levulinic Acid in Aqueous Media.* **Vinit Choudhary, Samir H. Mushrif, Christopher Ho, Andrzej Anderko, Vladimiros Nikolakis, Nebojsa S. Marinkovic, Anatoly I. Frenkel⊥, Stanley I. Sandler, and**

Dionisios G. Vlachos. 10, 2013, Journal of the American Chemical Society, Vol. 135, pp. 3997-4006.

42. *2,5-DMF production through hydrogenation of real and synthetic 5-HMF over transition metal catalysts supported on carriers with different nature.* **A Iriondo, A Mendiguren, M.B. Güemez, J. Requies, J.F. Cambra.** 2, Jabuary 2017, Catalysis Today, Vol. 279, pp. 286-295.

43. *Efficient Preparation of Liquid Fuel 2,5-Dimethylfuran from Biomass-Derived 5-Hydroxymethylfurfural over Ru–NaY Catalyst.* **Atul S. Nagpure, Nishita Lucas, and Satyanarayana V. Chilukuri.** 11, 2015, ACS Sustainable Chemistry & Engineering, Vol. 3, pp. 2909-2916.

44. *Production of Dimethylfuran from Hydroxymethylfurfural through Catalytic Transfer Hydrogenation with Ruthenium Supported on Carbon.* **Jungho Jae, Weiqing Zheng, Raul F. Lobo, Dionisios G Vlachos.** 7, July 2013, Chemistry and Sustainable Energy and Materials, Vol. 6, pp. 1158-1162.

45. *Hydrotalcite-supported gold-nanoparticle-catalyzed highly efficient base-free aqueous oxidation of 5-hydroxymethylfurfural into 2,5-furandicarboxylic acid under atmospheric oxygen pressure.* **Navneet Kumar Gupta, a Shun Nishimura,a Atsushi Takagakib and Kohki Ebitani.** 4, 2011, Green Chemistry, Vol. 13, pp. 824-827.

46. *A new approach for the production of 2,5-furandicarboxylic acid by in situ oxidation of 5-hydroxymethylfurfural starting from fructose.* **Kröger, M., Prüße, U. & Vorlop, KD.** 3, 2000, Topics in Catalysis, Vol. 13, pp. 237-242.

47. *Reaction of ketohexoses with acid in certain non-aqueous sugar solvents.* **C. J. Moye, R.J.Goldsack.** 7, July 1966, Journal of Chemical Technology and Biotechnology, Vol. 16, pp. 206-208.

48. *The formation of 5-hydroxymethylfurfural from hexoses.* **CJ, Moye.** 1966, Australian Journal of Chemistry, Vol. 19, pp. 2317-2320.

49. *Conversion of carbohydrates into 5-hydroxymethylfurfural catalyzed by ZnCl2 in water.* **Tiansheng Deng, Xiaojing Cui, Yongqin Qi, Yinxiong Wang, Xianglin Hou and Yulei Zhu.** 2012, Chemical Communications, Vol. 48, pp. 5494-5496.

50. *Conversion of carbohydrates and lignocellulosic biomass into 5-hydroxymethylfurfural using AlCl3·6H2O catalyst in a biphasic solvent system.* **Yu**

Yang, Chang-wei Hu and Mahdi M. Abu-Omar. 2, 2012, Green Chemistry, Vol. 14, pp. 509-513.

51. *Catalytic conversion of fructose and glucose into 5-hydroxymethylfurfural in hot compressed water by microwave heating.* **Xinhua Qi, Masaru Watanabe, Taku M. Aida, Richard L Smith Jr.** 13, 2008, Catalysis Communications, Vol. 9, pp. 2244-2249.

52. *Conversion of fructose to 5-HMF: a study on the behavior of heterogeneous cerium-based catalysts and their stability in aqueous media under mild conditions.* **Angela Dibenedetoo, Michele Aresta, Carlo Pastore, Luigi di Bitonto, Antonella Angelini and Eugenio Quaranta.** 2015, RSC Adv, Vol. 5, pp. 26941-26948.

53. *5-Hydroxymethylfurfural(HMF)- A Review Focussing on its manufacture.* **B.F.M.Kuster.** 8, 1990, Starch, Vol. 42, pp. 314-321.

54. **N, Lewis G.** *Valency and Structure of atoms and molceules.* New York : Wiley, 1923.

55. *Hard and Soft Acids and Bases.* **Pearson, Ralph G.** 22, 1963, Journal of the American Chemical Society, Vol. 85, pp. 3533-3539.

56. *A general perturbation treatment of chemical reactivity.* **Klopman, R.F. Hudson and G.** 12, 1967, Tetrahedron Letters, Vol. 8, pp. 1103-1108.

57. *Group theoretical classification of the tunneling–rotational energy levels of water dimer.* **Dyke, Thomas R.** 2, 1977, The Journal of Chemical Physics, Vol. 66, p. 492.

58. *Structures and vibrational spectra of water clusters in the self-consistent-field approximation.* **Leutwyler, R. Knochenmuss and S.** 7, 1992, The Journal of Chemical Physics, Vol. 96, p. 5233.

59. *Theoretical study of the (H2O)6 cluster.* **C.J. Tsai, K.D. Jordan.** 1-2, 1993, Chemical Physics Letters, Vol. 213, pp. 181-188.

60. *Water clusters.* **K.Liu, J.D.Cruzan and R.J.Saykally.** 1996, Science, Vol. 271, pp. 929-933.

61. *Lewis acid Catalysts stable in water: Correlation between catalytic activity in water and hydrolysis constants and exchange rate constants for substitution of inner-sphere ligands.* **Shu Kobayashi, Satoshi Nagayama and Tsuyoshi Busujima.** 1998, J.Am.Chem.Soc, Vol. 120, pp. 8287-8288.

62. *Effects of alkali metal halide salts on the hydrogen bond network of liquid water.* **Christopher D Cappa, Jared D Smith, Kevin R Wilson, Benjamin M Messer, Mary K Gilles, Ronald R Cohen and Richard J. Saykelly.** 2005, J.Phys.Chem. B, Vol. 109, pp. 7046-7052.

63. *The effect of dissolved halide anions on hydrogen bonding in liquid water.* **Jared D Smith, Richard J Saykally and Phillip L Geissler.** 2007, J.Am.Chem. Soc., Vol. 129, pp. 13847-13856.

64. *Review of hydrolysis behavior of ions in aqueous solutions.* **Jr, R.E.Mesmer and C.F.Baes.** s.l. : Materials Rseaerch Society, Mat.Res.Soc.Symp.Proc.Vol.180.

65. *Raman and infrared spectroscopy of carbohydrates: A review.* **Ewelina Wiercigroch, . Ewelina Szafraniec, Krzysztof Czamara, Marta Z Pacia, Katarzyna Majzner, Kamilia Kochan, Agnieszka Kaczor, Malgorzata Baranska, Kamilia Malek.** s.l. : Spectrochimica Acta Part A: Molecular and Biomolecular Spectroscopy, 2017, Vol. 185. 317-335.

66. *FTIR and laser-Raman spectra of oligosaccharides in water: characteriztion of the glycosidic bond.* **Marta Kacurakova, Mohamed Mathlouthi.** 1996, Carbohydrate Research, Vol. 284, pp. 145-157.

67. *Laser raman scattering of glucosamine N-acetylglucosamine, and glucuronic acid.* **C.Y.She, N.D.Dinh, Anthony T.Tu.** 2, s.l. : Biochimica et Biophysica Acta (BBA) - General Subjects, Vol. 372, pp. 345-357.

68. *Infrared and raman spectroscopy of carbohydrates : Part I: Identification of O□H and C□H-related vibrational modes for D-glucose, maltose, cellobiose, and dextran by deuterium-substitution methods.* **P.D.Vasko, J.Blackwell, J.L.Koenig.** 3, s.l. : Carbohydrate Research, October 1971, Vol. 19, pp. 297-310.

69. *Infrared and raman spectroscopy of carbohydrates. : Part II: Normal coordinate analysis of α-D-glucose.* **Vasko P.D, J. Blackwell, J.L.Koenig.** 3, August 1972, Carbohydrate Research, Vol. 23, pp. 407-416.

70. *Infrared and Raman spectra, conformational stability, ab initio calculations of structure, and vibrational assignment of α and β glucose.* **C.Araujo-Andrade, Facundo Ruiz, J.R.Martinez Mendoza, H.Terrones.** 2-3, February 2005, Journal of Molecular Structure: THEOCHEM, Vol. 714, pp. 143-146.

71. *Laser Raman Study of Solute-Solvent interactions in aqueous solutions of D-fructose, D-glucose and sucrose.* **Mathlouthi, Mohamed.** 1980, Carbohydrate Research, Vol. 81, pp. 213-223.

72. *Infrared and Raman Spectroscopy of Carbohydrates Part IV. Identification of configuration and conforation sensitive modes for D-glucose by normal coordinate analysis.* **John J Cael, Jack L.Koenig and John Blackwell.** 1974, Vol. 32, pp. 79-91.

73. *FTIR and laser-Raman spectra of oligosaccharides in water: Characterization of the glycosidic bond.* **Marta Kacurakova, Mohamed Mathlouthi.** 1996, Vol. 284, pp. 145-157.

74. *Fourier Transform IR and Raman Spectroscopy and structure of carbohydrates.* **R.G.Zhbankov, V.M.Andrianov, M.K.Marcheweka.** 1997, Vols. 436-437, pp. 637-654.

75. *Fourier Transform Infrared Spectroscopy as a Powerful Tool for the Study of Carbohydrates in Aqueous Solutions.* **D.M.Back, D.F.Michaelska, P.L.Polavarapu.** 2, 1984, Appplied Spectroscopy, Vol. 38, pp. 173-180.

76. *Analysis of structure and vibrational spectra of glucose and fructose.* **Medhat Ibrahim, Moussa Alaam, Hanan El-Haes, Abraham F. Jalbout, Aned de Leon.** 3, 2006, Ecletica Quimica, Vol. 31, pp. 15-21.

77. *Vibrational Assignments and isomerizationn rate constants from time dependent FTIR spectra of sugars.* **Polavarapu, Darlene M Back and Prasad L.** 1987, Carbohydrate Research, Vol. 165, pp. 173-187.

78. *Analysis of structure of the bands in the IR spectrum of beta-D-glucose by the regularized method of deconvolution.* **D.K.Buslov, N.A.Nikonenko, N.I.Sushko and R.G.Zhbankov.** 6, 2002, Journal of Applied Spectroscopy, Vol. 69.

79. *Vibrational Analysis of Aqueous Glucose Solutions. Temperature and Concentration Effects.* **Maria Elena Gallina, Paola Sassi, Marco Paolantoni, Assunta Morresi and Rosario Sergio Cataliotti.** 2006, J.Phys.Chem.B , Vol. 110, pp. 8856-8864.

80. *Improving ab initio infrared spectra of glucose-water complexes by considering explicit intermolecular hydrogen bonds.* **Sota, Teppei Suzuki and Takayuli.** 10133, s.l. : Journal of Chemical Physics, 2003, Vol. 119.

81. *Characteristics of hemicellulose, cellulose and lignin pyrolysis.* **Haiping Yanga, Rong Yanb, Hanping Chena, Dong Ho Leeb, Chuguang Zheng.** 12-13, 2007, Fuel, Vol. 86, pp. 1781-1788.

82. *Formation, molecular structure, and morphology of humins in biomass conversion: influence of feedstock and processing conditions.* **van Zandvoort, Wang Y, Rasrendra CB, van Eck ER, Bruijnincx PC, Heeres HJ, Weckhuysen BM.** 9, 2013, ChemSusChem, Vol. 6, pp. 1745-58.

83. *Catalytic conversion of glucose in dimethyl sulfoxide/water binary mixture chromium chloride: Rold of water on product distribution.* **Songyan Jia, Zhanwei Xu, Z.Conrad Zhang.** 2014, Chemical Engineering Journal, Vol. 254, pp. 333-339.

84. *Production and upgrading of 5-HMF using heterogeneous catalysts and biomass derived solvents.* **Jean Marcel R.Gallo, David Martin Alonso, Max A.Mellmer and James A.Dumesic.** 2013, Green Chemistry, Vol. 15, pp. 85-90.

85. *Efficient Isomerization of Glucose to Fructose over Zeolites in Consecutive Reactions in Alcohol and Aqueous Media.* **Shanmugavel Saravanamurugan, Marta Paniagua, Juan A.Melero and Andreas Riisager.** 14, 2013, J.Am.Chem.Soc, Vol. 135, pp. 5246-5249.

86. **Brittain E.F.H, George W.O and Wells C.H.J.** *Introduction to Molecular Spectroscopy.* London : Academic Press, 1975.

87. **Stuart, Barbara.** *Infrared Spectroscopy: Fundamentals and Applications.* s.l. : Wiley. p. 18.

88. **Stuart, B.** *Modern Infrared Spectroscopy.* Chichester : Wiley, 1996. Vol. ACOL series.

89. **Larkin, Peter J.** *Infrared and Raman Spectroscopy: Principles and Spectral Interpretation.* s.l. : Elsevier, 2011. p. 34.

90. *Reaction Induced Infrared Difference Spectroscopy for the study of protein reaction mechanism.* **Barth, Christian Zscherp and Andreas.** 7, 20 February 2001, Biochemistry, Vol. 40, pp. 1875-1883.

91. *ATP-induced phosphorylation of the sarcoplasmic reticulum Ca 2+ ATPase: molecular interpretation of infrared difference spectra.* **A Barth, W Mäntele.** 1, 1998, Biophysical journal, Vol. 75, pp. 538-544.

92. *Changes of protein structure, nucleotide microenvironment, and Ca 2+-binding states in the catalytic cycle of sarcoplasmic reticulum Ca 2+-ATPase: investigation of nucleotide binding, phosphorylation and phosphoenzyme conversion by FTIR difference spectro.* **A Barth, W Kreutz, W Mäntele.** 1, 1994, Biochimica et Biophysica Acta (BBA)-Biomembranes, Vol. 1194, pp. 75-91.

93. *Effect of Hydrophobicity of Amino Acids on the Structure of Water.* **Makoto Ide, Yasushi Maeda , and Hiromi Kitano.** 35, 1997, Journal of Physical Chemistry B, Vol. 101, pp. 7022-7026.

94. *Urea and urea–water solutions—an infrared study.* **Jože Grdadolnika, Yves Maréchalb.** 1-3, 2002, Journal of Molecular Structure, Vol. 615, pp. 177-189.

95. *Hydroxymethylfurfural, A versatile Platform Chemical Made from Renewable Resources.* **Robert- Jan van Puetten, Jan C. van der waal, Ed de Jong, Carolus B Rasendra, Hero J Heeres and Johannes G de Vries.** 3, 2013, Chemical Reviews, Vol. 113, pp. 1499-1597.

96. *Greener Solvents for Making Chemicals from Biomass* . **Barros, José.** 30 May 2016, ACS.

97. *Formation, Molecular Structure, and Morphology of Humins in Biomass Conversion: Influence of Feedstock and Processing Conditions.* **van Zandvoort, Wang Y, Rasrendra CB, van Eck ER, Bruijnincx PC, Heeres HJ, Weckhuysen BM.** 9, 2013, Vol. 6, pp. 1745-58.

98. *Aluminum Chloride: A highly effectuve catalyst for addition of amines to carbodiimides to synthesize substituted guanidines.* **ZHU XueHua, Xu Fan, Shen Qi.** 26, 2012, Chinese Science Bulletin, Vol. 57.

99. *Kinetic Parameters for the noncatalyzed and Enzyme Catalyzed Mutarotation of glucose using a blood glaucometer.* **John R.Hardee, Bryan Delegado and Wray Jones.** 2011, Journal of Chemical Education, Vol. 88, pp. 798-800.

100. *Kinetics of glucose isomerization to fructose by immobilized glucose isomerase: anomeric reactivity of d-glucose in kinetic model.* **Hong, Han Seung Lee and Juan.** 2, 2000, Journal of Biotechnology, Vol. 84, pp. 145-153.

101. *Hidden isobestic points in Ultraviolet Spectra.* **Pouet MF, Baures E, Vaillant S, Thomas O.** 4, April 2004, Applied Spectroscopy, Vol. 58, pp. 486-498.

102. *Review of hydrolysis of ions in aqueous solutions.* **Jr, R.E.Mesmer and C.F.Baes.** s.l. : Mat.Res.Soc.Symp.Proc.Vol180.

103. *Lewis Acid Catalysts Stable in Water. Correlation between Catalytic Activity and Hydrolysis Constants and Exchange Rate Constants for Substitution of Inner-Sphere water ligands.* **Shu Kobayashi, Satoshi Nagayama and Tsuyoshi Basujima.** s.l. : J.Am.Chem.Soc.1998,120,8287-8288, 1998, Vol. 120.